Thesis for the degree of Licentiate of Engineering in
Machine and Vehicle Systems

Haptic Feedback Control Methods for Steering Systems

TUSHAR CHUGH

Department of Mechanics and Maritime Sciences
Vehicle Engineering and Autonomous Systems
CHALMERS UNIVERSITY OF TECHNOLOGY
Göteborg, Sweden 2019

Haptic Feedback Control Methods for Steering Systems
TUSHAR CHUGH

Thesis for the degree of Licentiate of Engineering 2019:05
Department of Mechanics and Maritime Sciences
Chalmers University of Technology
SE–412 96 Göteborg
Sweden
Telephone: +46 (0)31–772 1000

Chalmers Reproservice
Göteborg, Sweden 2019

"Being second is to be the first of the ones who lose."

Ayrton Senna

Haptic Feedback Control Methods for Steering Systems

Tushar Chugh
Department of Mechanics and Maritime Sciences
Chalmers University of Technology

Abstract

Haptic feedback from the steering wheel is an important cue that defines the steering feel in the driver-vehicle interaction. The steering feedback response in an electric power assisted steering is primarily dependent on its control strategy. The conventional approach is open loop control, where different functions are implemented in a parallel structure. The main drawbacks are: (a) limited compensation of the hardware impedance, (b) hardware system dependent steering feedback response and (c) limitation on vehicle motion control request overlay. This thesis investigates closed-loop control, in which the desired steering feedback response can be separated from the hardware dynamics. Subsequently, the requirements can be defined at the design stage.

The closed-loop architecture constitutes of a higher and lower level controller. The higher level control defines the reference steering feedback, which should account for both driver and road excitation sources. This thesis focuses on the driver excitation, where a methodology is proposed for developing such a reference model using the standard vehicle handling maneuvers. The lower level control ensures: (a) reference tracking of the higher level control, (b) hardware impedance compensation and (c) robustness to unmodeled dynamics. These interdependent objectives are realized for a passive interaction port driving admittance. The two closed-loop possibilities, impedance (or torque) and admittance (or position) control, are compared objectively. The analysis is further extended to a steer-by-wire force-feedback system; such that the lower level control is designed with a similar criteria, keeping the same higher level control.

The admittance control is found limited in performance for both the steering systems. This is explained by a higher equivalent mechanical inertia caused by the servo motor and its transmission ratio in electric power assisted steering; and for steer-by-wire force-feedback, due to the uncertainty in drivers' arm inertia. Moreover, it inherently suffers from the conflicting objectives of tracking, impedance compensation and robustness. These are further affected by the filtering required in the admittance lower level control. In impedance control, a better performance is exhibited by its lower level control. However, the required filtering and estimation in the impedance higher level control is its biggest disadvantage. In closed-loop setting, the angular position overlay with a vehicle motion control request is also relatively easier to realize than open loop.

Keywords: Haptic feedback, steering system, impedance and admittance control, passivity and coupled stability, torque and position overlay, system identification

Acknowledgments

I take this opportunity to express my sincere gratitude and appreciation to my academic supervisor Dr. Fredrik Bruzelius for his exceptional guidance, sharing his knowledge and time. I am grateful to my industrial supervisor Dr. Matthijs Klomp for his genuine feedback on my work and also for initiating this project. I am further thankful to my examiner Prof. Bengt Jacobson for supervising on a higher level and asking the fundamental questions. I would also like to acknowledge Dr. Barys Shyrokau for our cooperation and providing me with the measurement equipment. Thank you to Dr. Mathias Lidberg and Dr. Shenhai Ran for their supervision during the first year of this project. This thesis would not have been possible without our funding partners; ITEAM project in the European Union's Horizon 2020 research and innovation program and VINNOVA of the Fordonsstrategisk forskning och innovation (FFI).

At Volvo Car Corporation, I would like to thank my manager Georgios Minos for the administrative support and my colleagues Alejandro González, Anton Albinsson, Carl-Johan Häll, David Dahlgren, Håkan Karlsson and Joakim Norrby for all the help over these years. I would like to appreciate, in particular, my colleague Pontus Carlsson for helping me with the prototype vehicle, technical and non-technical discussions we have had in the last two years.

In my division at Chalmers University of Technology, I am thankful to Britta, Simone and Sonja for taking care of the important administrative things. I would like to complement my fellow PhD students from all the groups for creating a friendly work environment. Special thanks to my former and present colleagues: Adi, Leon, Pär, Randi, Sina, Toheed and Weitao for all the good times.

Finally, I would like to thank my family: my parents, grandparents and my brother, for their continuous support throughout this time and keeping the faith in me.

Tushar Chugh
Göteborg, May 2019

Nomenclature

Symbol	Description
C_{α_f}	Front axle tire cornering stiffness
C_{α_r}	Rear axle tire cornering stiffness
F_{assist}	Steering rack assist force
$F_{bn,fric}$	Friction force on EPAS motor ball-nut assembly
F_{ext}	Disturbance force on steering rack
F_{rack}	Steering rack force from tire and wheel kinematics
$F_{rack,ext}$	External steering rack force from road
F_{tb}	Torsion bar force on steering rack
F_{xf}, F_{xr}	Front and rear axle longitudinal force
F_{yf}, F_{yr}	Front and rear axle lateral force
G_{22}, G_{32}	Motor torque to angular position and torsion bar torque function
G_{arm}	Driver arm admittance
G_{load}	System load transfer function
$H_{fb,M}$	Impedance feedback transfer function
$H_{fb,\theta}$	Admittance feedback transfer function
$H_{ref,M}$	Impedance reference transfer function
$H_{ref,\theta}$	Admittance reference transfer function
H_{servo}	Servo closed-loop transfer function
J_{arm}	Driver arm inertia
J_{mot}	Servo motor inertia
J_{pin}	Pinion inertia
J_{rb}	EPAS motor recirculating balls' inertia
J_{ref}	Reference inertia
J_s	Steering wheel and column inertia
J_z	Vehicle yaw inertia
L_d	Interaction port driving admittance loop gain
L_M	Impedance control loop gain
L_θ	Admittance control loop gain
M_{arm}	Driver arm torque
$M_{ext,req}$	External motor torque overlay request
M_{mot}	Actual servo motor torque

Symbol	Description
$M_{mot,eff}$	EPAS motor effective torque on pinion
$M_{mot,ext}$	EPAS motor torque request from vehicle motion control
$M_{mot,req}$	EPAS motor torque request from steering feedback control
$M_{pin,fric}$	Friction torque on pinion
M_{rack}	Torque translated from steering rack force on pinion
$M_{rb,fric}$	EPAS motor recirculating ball friction torque
M_s	Steering torque
$M_{s,fric}$	Friction torque on steering wheel
M_{steer}	Steer torque from the tire about the steering axis
M_{tb}	Torsion bar torque
$M_{tb,ref}$	Reference torsion bar torque
T_{α_f}	Front axle tire relaxation time constant
T_{α_r}	Rear axle tire relaxation time constant
U	Input signal transfer function
Y	Output signal transfer function
Y_k	k^{th} output signal transfer function
$Y_{k,ref}$	k^{th} reference signal transfer function
Z	Driving port admittance transfer function
b_{mot}	Servo motor viscous damping
b_{pin}	Pinion viscous damping
b_{ref}	Reference viscous damping
b_s	Steering viscous damping
c_{arm}	Driver arm stiffness
c_{belt}	EPAS motor belt stiffness
c_{bn}	EPAS motor ball-nut stiffness
c_{rack}	Steering rack stiffness
c_{rb}	EPAS motor recirculating balls' stiffness
c_{ref}	Reference stiffness
c_{tb}	Torsion bar stiffness
e_M	Error in torque
$e_\theta, \dot{e}_\theta, \ddot{e}_\theta$	Error in angular position, velocity and acceleration
e_{Y_k}	Error in k^{th} output variable
f_{in}	Frequency in Hz
i_{belt}	EPAS motor to pulley belt transmission ratio
i_{mp}	EPAS motor to pinion transmission ratio
i_{mr}	EPAS motor to rack transmission ratio
i_{rp}	Steering rack to pinion gear ratio
i_s	Overall steering pinion to road wheel angle ratio
j	Complex operator
k_{arm}	Driver arm damping

Symbol	Description
k_{belt}	EPAS motor belt damping
k_{bn}	EPAS motor ball-nut damping
$k_{eq,rack}$	EPAS equivalent rack viscous damping
k_{rack}	Steering rack viscous damping
k_{rb}	EPAS motor recirculating balls' damping
k_{ref}	Reference damping
k_{tb}	Torsion bar viscous damping
l_f	Distance from vehicle's center of gravity to front axle
l_r	Distance from vehicle's center of gravity to rear axle
m	Vehicle mass
m_{bn}	EPAS motor recirculating balls' mass
$m_{eq,rack}$	EPAS equivalent rack mass
m_{rack}	Steering rack mass
n_{mech}	Steering caster trail
n_{tire}	Tire pneumatic trail
n_{total}	Total steering trail
s	Laplace operator
t	Time domain operator
v_x	Vehicle longitudinal velocity
v_y	Vehicle lateral velocity
$x_{bn}, \dot{x}_{bn}, \ddot{x}_{bn}$	EPAS ball-nut position, velocity and acceleration
$x_{rack}, \dot{x}_{rack}, \ddot{x}_{rack}$	Steering rack position, velocity and acceleration
$\mathbf{0}_{n\times m}$	$n \times m$ null matrix
$\mathbf{A}$	System state matrix
$\mathbf{B}$	System input-to-state matrix
$\mathbf{C}$	System state-to-output matrix
$\mathbf{D}$	System feedthrough matrix
$\mathbf{G}$	Output transfer function matrix
$\mathbf{G}_a$	Approximated model output transfer function matrix
$\mathbf{I}_{n\times n}$	$n \times n$ identity matrix
$\mathbf{u}$	System input vector
$\mathbf{x}$	System state vector
$\mathbf{y}$	System output vector
$\alpha_0, \alpha_1, \alpha_1'$	Impedance feedback control gains
α_f, α_r	Front and rear axle lateral slip angle
β	Body sideslip angle
$\beta_0, \beta_1, \beta_2, \beta_3$	Admittance feedback control gains
$\delta, \dot{\delta}$	Road wheel angle and velocity
$\theta_{ext,req}$	External position request from vehicle motion control
$\theta_{mot}, \dot{\theta}_{mot}, \ddot{\theta}_{mot}$	Motor angular position, velocity and acceleration

Symbol	Description
$\theta_{mot,ref}$	Reference motor angular position
$\theta_{pin}, \dot{\theta}_{pin}, \ddot{\theta}_{pin}$	Pinion angular position, velocity and acceleration
$\theta_{pin,ref}$	Reference pinion angular position
$\theta_{rb}, \dot{\theta}_{rb}, \ddot{\theta}_{rb}$	EPAS recirculating ball position, velocity and acceleration
$\theta_s, \dot{\theta}_s, \ddot{\theta}_s$	Steering angular position, velocity and acceleration
$\theta_{s,req}, \dot{\theta}_{s,req}$	Driver requested steering angular position and velocity
σ_i	i^{th} *Hankel* Singular value
$\sigma_{\alpha_f}, \sigma_{\alpha_r}$	Front and rear axle tire relaxation length
τ	Integrator time step
ϕ_m	Phase margin
$\dot{\psi}, \ddot{\psi}$	Vehicle yaw rate and acceleration
ω, ω_{in}	Frequency

All quantities are given in SI units and angles in radians, unless stated otherwise.

Thesis

The thesis consists of an extended summary of the research work and the following appended papers:

(A) Chugh, T., Chen, W., Klomp, M., Ran, S. and Lidberg, M., *Design and Control of Model Based Steering Feel Reference in an Electric Power Assisted Steering System.* In: Proceedings of the 25th International Symposium on Dynamics of Vehicles on Roads and Tracks (IAVSD), Rockhampton, Australia, pp. 43–49, 2017

(B) Chugh, T., Bruzelius, F., Klomp, M. and Ran, S., *Comparison of Steering Feel Control Strategies in Electric Power Assisted Steering.* In: Proceedings of the 14th International Symposium on Advanced Vehicle Control (AVEC), Beijing, China, 2018

(C) Chugh, T., Bruzelius, F., Klomp, M. and Shyrokau, B., *Design of Haptic Feedback Control for Steer-by-Wire.* In: Proceedings of the 21st IEEE International Conference on Intelligent Transportation Systems (ITSC), Maui, USA, pp. 1737–1744, 2018

(D) Chugh, T., Bruzelius, F., Klomp, M. and Shyrokau, B. *An Approach to Develop Haptic Feedback Control Reference for Steering Systems Using Open-loop Driving Maneuvers.* **Manuscript submitted** to Vehicle System Dynamics on Apr. 7, 2019.

The author of this thesis was responsible for modeling, simulation, experiments, analysis and writing the papers. The co-authors contributed with technical discussions, supervision and revision of the manuscripts. Paper B, Paper C and Paper D were written by the author with valuable inputs from the co-author, Dr. Fredrik Bruzelius.

Table of Contents

1 Introduction **1**
- 1.1 Background . . . 1
- 1.2 Research questions . . . 2
- 1.3 Contribution . . . 3
- 1.4 Limitations . . . 4
- 1.5 Thesis outline . . . 5

2 System dynamics and modeling **7**
- 2.1 Steering system . . . 7
  - 2.1.1 Electric power assisted steering model . . . 8
  - 2.1.2 Steer-by-wire force-feedback model . . . 11
- 2.2 Vehicle model . . . 12
- 2.3 Muscular driver arm model . . . 14

3 Interaction between driver and steering **15**
- 3.1 State-of-the-art: Open loop . . . 16
  - 3.1.1 Electric power assisted steering control . . . 16
  - 3.1.2 Force-feedback control . . . 21
- 3.2 Introduction to Closed-loop . . . 23
  - 3.2.1 Impedance and Admittance control . . . 23
  - 3.2.2 Coupled stability analysis . . . 24
  - 3.2.3 Feedback control validation . . . 36
  - 3.2.4 Reference model for driver excitation . . . 36
  - 3.2.5 Reference model for road excitation: The step forward . . . 41

4 Overlaying vehicle motion control request **43**
- 4.1 Open loop motor torque overlay . . . 43
- 4.2 Closed-loop angular position overlay . . . 45

5 Summary **47**
- 5.1 Discussion and conclusion . . . 47
- 5.2 Future work . . . 49

Bibliography 51

APPENDED PAPERS

Chapter 1

Introduction

The literal meaning of the term 'haptics' is touch feedback, which defines the interaction between a human, machine and environment in a mechatronic system. This can be further categorized in kinesthetic and tactile feedback. The kinesthetic feedback deals with the muscular forces and positioning of the body joints, whereas the sensation affecting the skin, for example temperature change, falls under tactile feedback. The importance of haptic feedback is not something new, see e.g. [46]. This is acknowledged in different applications, for example in teleoperated systems [6, 32, 33, 38, 47], surgical robots [35, 45], flight simulators [15, 16, 25], etc. This thesis studies the role of (kinesthetic) haptic feedback in vehicle steering systems.

The driver-vehicle interaction is subjectively perceived by humans as steering feel. The term 'steering feel' is an amalgamation of multiple feedback cues, such as haptic, optical, acoustic, motion, etc. With an advancement of the automotive industry in the recent years due to electrification and software, the passenger car steering systems have gradually transformed from hydraulic to electric power assisted steering. In the latter, the servo motor is primarily responsible for the 'haptic' part of the steering feel. For a relevant human-machine interface, the haptic feedback from the steering wheel is a very important element for the drivers. This thesis focuses on the haptic (or steering) feedback control for such systems.

1.1 Background

The transition from hydraulic power assisted steering (HPAS) to electric power assisted steering (EPAS) is driven by various aspects, such as cost, packaging, environment reasons, etc. The environmental benefit of EPAS, comes from its power-on demand[1] capability. This directly influences the reduction in fuel consumption and subsequently lower CO_2 emissions. These claims can be found in, e.g. 10% reduction for an average fuel consumption of 7.7 l/100km in a two-liter gasoline engine [8], 16.1 g/km less CO_2

[1]Energy consumption only during steering and not while driving straight ahead.

emissions as compared to HPAS [7], reduction by 4.1% in urban driving cycle [20], also qualitatively in [26], etc. Apart from the fuel consumption improvement in EPAS, the electrical actuation opens the door for many other functions related to steering feedback control, vehicle safety and driving assistance [23].

The paradigm shift towards driving automation has made the servo motor an actuator for vehicle motion control. This is exemplified in lane keeping aid functions. In EPAS, a single actuator is responsible for both the tasks; haptic feedback and vehicle motion control. As a result, there will always be a compromise under certain situations attributed to the prioritization of the control objective. A possible solution in the future could be to have two separate actuators, like in a steer-by-wire (SbW) system. In short, the steering wheel is mechanically decoupled from the road wheels; the steering wheel and road wheel actuators are connected to each subsystem respectively, to fulfill the required tasks. The importance of haptic feedback in steering is illustrated here using two simple examples. Firstly, [39] showed an improvement in the drivers' steering response by including the lateral acceleration feedback to manipulate the steering torque for preventing the rollover situation. The second example deals with a racing scenario, where higher cornering speeds are required for shorter lap times. This is possible by maximizing the tire-road grip potential and operating near to the road friction limits. As a consequence, the actual trajectory deviations from the optimal racing line are much narrower. This demands for a higher steering activity from the racing drivers near the limit in search of maximum tire-road grip as experimentally shown in [43]. A similar conclusion can be drawn from [42], an increased compensatory steering control of the racing driver model results is a faster lap. In reality, the racing driver could increase the steering activity near the handling limits, if and only if the tire-road feedback effects on the steering wheel are sufficient and transmitted with a faster response.

In state-of-the-art EPAS control (see e.g. [3, 9, 23, 29]), the external road feedback is mechanically filtered more aggressively than HPAS due to additional (equivalent) servo motor impedance. And this is one its biggest drawback for causing an attenuation of the high frequency road feedback (despite comprising the existing steering feedback control functions). Similarly in state-of-the-art SbW-FFb (see e.g. [5, 19, 24]), the haptic response is compromised because of two reasons: (a) the servo motor impedance and (b) missing external road feedback information. For road feedback information in SbW-FFb, it must be estimated using some control algorithms. The problem of additional mechanical servo motor dynamics (or hardware impedance) on steering feedback is objectively explained later in Chapter 3. The following subsection on research questions is formulated based on the need of improving the state-of-the-art (open loop) steering feedback control for a desired haptic response.

1.2 Research questions

The aim of this research work is to investigate the possibility of applying the closed-loop haptic feedback control setting to EPAS and SbW-FFb. In these approaches, we define

a lower and higher level control. The lower level control forms the closed-loop system with the hardware setup, ensuring a sufficient performance, stability and robustness in terms of a given control variable. The higher level control consists of the desired steering feedback response, which provides a reference variable to the lower level control.

There are three explicit problems for our research work. The first question is addressed towards the higher level control for a reference steering feedback response. The next question is to define the lower level control for the given cases, EPAS and SbW-FFb, on the criteria of reference tracking, hardware impedance compensation and robustness. The last question is regarding the interface of overlaying the two functionalities, haptic feedback control and vehicle motion control. These questions are briefly stated as follows.

(a) How to represent the steering feedback response using a model-based (control) reference with different excitation sources?

(b) What are the closed-loop possibilities depending on the feedback control variable for electric power assisted steering and steer-by-wire force-feedback? How to objectively compare their performance following a defined stability criteria?

(c) How to overlay the request from haptic feedback control and vehicle motion control functions in closed-loop setting, and what should be the interfacing variable?

1.3 Contribution

The contribution of our work is finding the answers to the above mentioned research questions. This can be summarized as follows.

I. In electric power assisted steering system, the effect of higher mechanical impedance on the steering rack due to servo motor and its transmission ratio is investigated. A higher dependency on the impedance (or inertia) compensation function in open loop control is likely to have stability issues for such hardware systems. This is due to typical signal processing for an estimated angular acceleration (*Paper A*). To overcome the hardware impedance using the closed-loop setting, a fair comparison between the two lower level control possibilities, impedance and admittance control, is further investigated. A sufficient linear feedback control law is formulated with an assumption of a given higher level control. The controller parameters are selected to ensure uncoupled and coupled stability of the interconnected system. The lower level admittance control results in an inferior performance (in comparison to the impedance control) due to higher equivalent rack (or hardware) impedance (*Paper B*). A generalized conclusion for such systems could be, '*the position reference tracking objective could conflict with the hardware impedance compensation objective for maintaining a desired stability and robustness criteria of the closed-loop system*'.

II. In the second case, a steer-by-wire force-feedback system is under consideration. The effect of FFb-motor impedance could affect the open loop steering feedback response due to additional dynamics (if the effective inertia is higher). To overcome the compromised open loop reference tracking, the closed-loop control methods are compared and further analyzed using the same criteria as before. With a sufficient linear feedback (lower level) control and a given higher level control, the uncoupled and coupled stability of the interconnected system is guaranteed. The performance of the lower level admittance control is affected by the uncertainty in driver arm inertia. Because higher arm inertia in FFb systems results in a loss of closed-loop performance and robustness (*Paper C*). The generalized conclusion on the lower level control from before is also valid here.

III. A methodology is presented for extracting the (steering feedback) reference model parameters for driver excitation using the open loop vehicle handling maneuvers in both steady state and transient. It consequently results in a sequentially structured impedance and admittance reference for the higher level control. This inertia-spring-damper-friction haptic feedback reference model can be implemented for closed-loop steering systems (*Paper D*). The performance of the impedance reference is compromised as compared to the admittance reference because of the estimation of angular acceleration signal.

IV. The angular position overlay in closed-loop setting can be used to realize the vehicle motion control interventions via the haptic feedback control. This has two advantages: (a) a better transition in steering torque response as compared to the motor torque overlay in open loop and (b) realization of the vehicle motion control request without driver-in-the-loop (although low frequency inputs only) with the same controller.

1.4 Limitations

Some of the main limitations from this thesis are also highlighted.

(a) For lower level control, the feedback laws assume a linear time invariant (LTI) system. The derived uncoupled stability conditions consider useful simplifications (for example highly stiff torsion bar, neglecting smaller terms, etc.); these are mentioned throughout the chapters respectively. For coupled stability analysis, the model of driver arm mechanics is considered to be passive.

(b) Consideration of feedforward control (as an additional degree of freedom for the lower level control) in the closed-loop possibility is kept out of context. Because it does not affect the closed-loop stability analysis anyhow and it improves the initial response only.

(c) The higher level control is limited to the driver excitation only (and also within the linear vehicle handling range). The inclusion of road excitation for the higher level control is not discussed in this thesis.

(d) For overlaying the haptic feedback control with a vehicle motion control request, we have compared the straightforward possibilities; motor torque overlay in open loop and angular position overlay in closed-loop. There could be other possible combinations, but we have not considered them for simplicity.

1.5 Thesis outline

The presented chapters provide a detailed overview of the research that has been done. They are further appended with the papers as mentioned before. The complete thesis in itself is self-contained for understanding the topic.

The thesis is organized as follows: Chapter 2 describes the system dynamics and modeling of EPAS and SbW-FFb, along with the simplified models of vehicle and muscular driver arm mechanics. Chapter 3 covers the interaction dynamics between the driver, steering and vehicle with open and closed-loop haptic feedback control methods. The closed-loop (feedback) control is designed using a thorough stability analysis and its criteria as explained in this chapter. A very brief discussion on the possibility of overlaying the request from haptic feedback control and vehicle motion control is done in Chapter 4. Last but not the least, Chapter 5 summarizes the work with a discussion, conclusion and future work.

Chapter 2

System dynamics and modeling

In this chapter, a brief introduction to the steering system and its interaction with the vehicle and driver is given. The relevant system dynamics, for the haptic feedback controller design, is mathematically formulated using simplified models. The undertaken modeling assumptions, for representing this mechanical interaction, are also motivated.

2.1 Steering system

The focus of this thesis is on electric power assisted steering and steer-by-wire force-feedback. The respective layouts are shown in Fig. 2.1 including some of the other main components. In EPAS, there is a mechanical connection to the road wheels. The steering rack mounted servo motor is responsible for providing the required assistance to overcome the steering rack force. Whereas in SbW system, this mechanical connection between the driver (via steering wheel) and steering rack is not available. Subsequently, the hardware consists of two actuators for controlling the road wheels (via steering rack) and steering wheel respectively. The lower actuator is mainly responsible for vehicle handling and its positioning on the road, while the upper actuator ensures the required drivers' haptic feedback. For SbW, the thesis focuses on the latter. This FFb motor generates the complete haptic feedback, unlike the torque support provided in EPAS [9, 17, 23, 28]. In a conventional state-of-the-art steering system (for instance in EPAS), there are three primary sources of excitation; driver, environment and vehicle. The driver excitation involves human initiated steering movements. The external road inputs are an important environmental excitation source. And finally, the vehicle interventions from driving-steering assistance (or vehicle motion control) functions such as haptic guidance, lane keeping aid, etc. Depending on the driving behavior, requirements and application, the definition of "good" steering feel varies. An appropriate steering feedback is required not only during the driver excitation. For high performance vehicles, for example in racing applications, the external road excitation becomes critical. Because the racing driver relies on this information, to follow the optimal racing line as explained in Section 1.1. On the contrary, it is also understandable to attenuate the

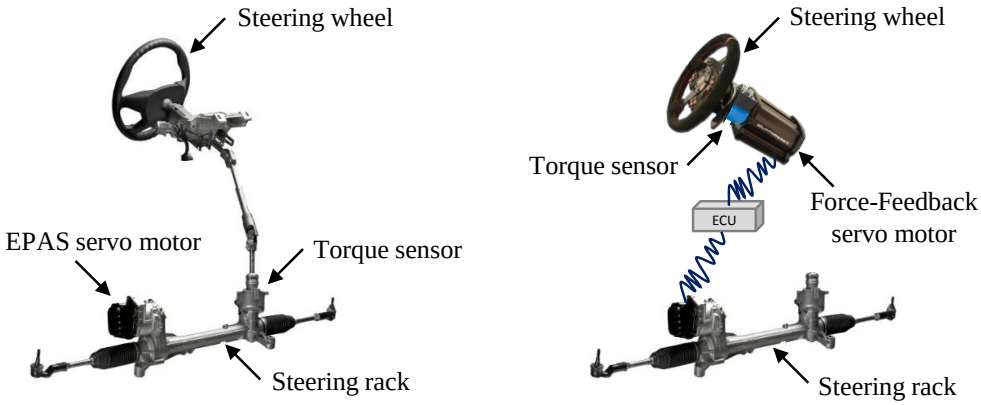

(a) Electric Power Assisted Steering (b) Steer-by-Wire

Figure 2.1: *The two steering layouts under consideration are (a) electric power assisted steering and (b) steer-by-wire.*

unwanted steering disturbances; for example while driving on the rough road [44]. This should be achieved with similar steering performance in SbW-FFb. Nevertheless, the phenomenon of external road excitation (and its feedback) does not exist in SbW, and needs to be realized.

The following subsections model the system hardware with different levels of complexity, for an analytical comparison and performance evaluation of the haptic feedback control methods in Chapter 3.

2.1.1 Electric power assisted steering model

The actual inputs to the steering system are steering torque from the driver (M_s), steering rack assist force (F_{assist}) translated from the motor torque (M_{mot}) and rack force from the tie-rods (F_{rack}). Keeping this in context, the simplified steering model is shown in Fig. 2.2. Here, the resulting force balance on the steering rack is translated to moment balance on the pinion using the pinion-to-rack transmission ratio, i_{rp}. The equations of motion are as follows, with effective motor torque as $M_{mot,eff} = F_{assist}/i_{rp}$.

$$\begin{aligned} J_s\ddot{\theta}_s &= -b_s\dot{\theta}_s - M_{tb} - M_{s,fric} + M_s \\ J_{pin}\ddot{\theta}_{pin} &= -b_{pin}\dot{\theta}_{pin} + M_{tb} - M_{rack} - M_{pin,fric} + M_{mot,eff} \\ \text{where } M_{tb} &= k_{tb}(\dot{\theta}_s - \dot{\theta}_{pin}) + c_{tb}(\theta_s - \theta_{pin}) \text{ and } M_{rack} = F_{rack}/i_{rp} \end{aligned} \tag{2.1}$$

The steering system is mechanically coupled to the EPAS motor. Here the motor dynamics is considered separately. The hardware causality of motor to steering rack interaction (with F_{assist} and $\dot{x}_{rack}$ towards the steering rack and EPAS motor respectively) can be seen in Fig. 2.3 with the equations of motion in Eq. (2.2), such that $F_{assist} = k_{bn}(\dot{x}_{bn} - \dot{x}_{rack}) + c_{bn}(x_{bn} - x_{rack})$. For a simplified analysis and real-time

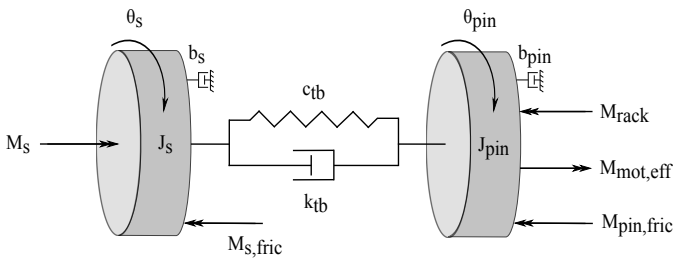

Figure 2.2: *Free body diagram of a simplified electric power assisted steering system with 2-DOF (degree of freedom); steering angle and pinion angle (or equivalent to rack displacement).*

controller implementation, the model order is reduced due to high stiffness components.

$$\begin{aligned} J_{mot}\ddot{\theta}_{mot} =& - b_{mot}\dot{\theta}_{mot} - k_{belt}(\dot{\theta}_{mot} - \dot{\theta}_{rb}i_{belt}) - c_{belt}(\theta_{mot} - \theta_{rb}i_{belt}) \\ &+ M_{mot} \\ J_{rb}\ddot{\theta}_{rb} =& - k_{rb}(\dot{\theta}_{rb}i_{rb} - \dot{x}_{bn})i_{rb} - c_{rb}(\theta_{rb}i_{rb} - x_{bn})i_{rb} + k_{belt}(\dot{\theta}_{mot} \\ &- \dot{\theta}_{rb}i_{belt})i_{belt} + c_{belt}(\theta_{mot} - \theta_{rb}i_{belt})i_{belt} - M_{rb,fric} \\ m_{bn}\ddot{x}_{bn} =& - k_{rb}(\dot{x}_{bn} - \dot{\theta}_{rb}i_{rb}) - c_{rb}(x_{bn} - \theta_{rb}i_{rb}) - F_{bn,fric} - F_{assist} \end{aligned} \tag{2.2}$$

For model order reduction, we take a simple case study where the motor is coupled to steering rack with an external compliance (c_{rack} and k_{rack}) and a force component, $F_{ext} = F_{tb} + F_{rack,ext}$. Neglecting friction from Eq. (2.2) and including $m_{rack}\ddot{x}_{rack} = -k_{rack}\dot{x}_{rack} - c_{rack}x_{rack} + F_{ext} + F_{assist}$, the state-space form can be written as:

$$\begin{aligned} \dot{\mathbf{x}} &= \mathbf{A}\mathbf{x} + \mathbf{B}\mathbf{u} \\ \mathbf{y} &= \mathbf{C}\mathbf{x} + \mathbf{D}\mathbf{u} \\ \text{where, } \mathbf{x} &= [\theta_{mot}\ \dot{\theta}_{mot}\ \theta_{rb}\ \dot{\theta}_{rb}\ x_{bn}\ \dot{x}_{bn}\ x_{rack}\ \dot{x}_{rack}]^T, \\ \mathbf{y} &= x_{rack} \text{ and } \mathbf{u} = [M_{mot}\ F_{ext}]^T. \end{aligned} \tag{2.3}$$

The approximated (lower order) model assumes a rigid servo motor to rack connection; thus implying $\dot{x}_{rack} = \dot{\theta}_{mot}/i_{mr}$ and $F_{assist} = M_{mot}i_{mr}$, where $i_{mr} = i_{belt}/i_{rb}$. Hence, the resulting equation of motion is given below. The outcome is amplification of steering rack (hardware) impedance due to servo motor and its transmission ratios.

$$\begin{aligned} m_{eq,rack}\ddot{x}_{rack} &= -k_{eq,rack}\dot{x}_{rack} - c_{rack}x_{rack} + F_{ext} + F_{assist} \\ \text{where, } m_{eq,rack} &= m_{rack} + m_{bn} + J_{mot}i_{mr}^2 + J_{rb}/i_{rb}^2 \text{ and } k_{eq,rack} = k_{rack} + b_{mot}i_{mr}^2 \end{aligned} \tag{2.4}$$

The Laplace transform of a state-space gives $Y(s) = \mathbf{G}(s)U(s)$, such that $\mathbf{G}(s) = \mathbf{C}(s\mathbf{I}-\mathbf{A})^{-1}\mathbf{B}+\mathbf{D}$. The singular values of $\mathbf{G}(s)$, as defined in [41, pp. 72–79], are shown on a frequency plot in Fig. 2.4(a) for full and reduced order models. The optimal *Hankel* model (as a 2^{nd} order approximation) is also included for reference. The corresponding

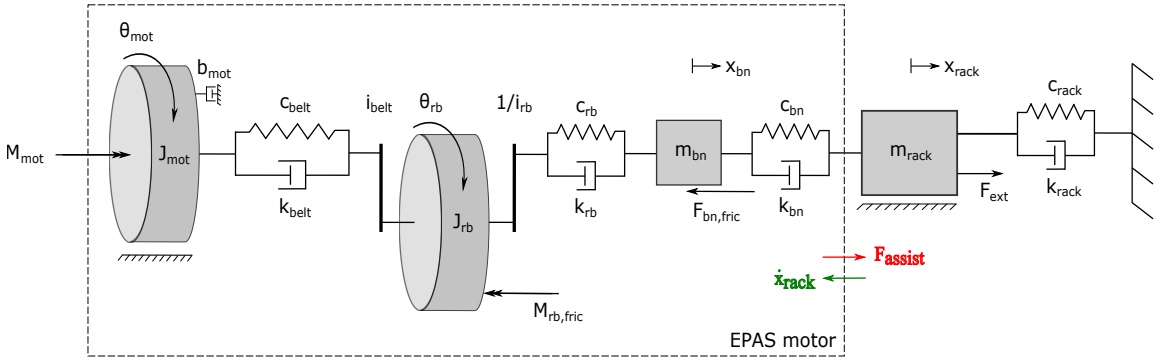

Figure 2.3: *Free body diagram showing the mechanical interaction between the subsystems; electric power assisted steering motor and steering rack. The motor model has 3-DOF; motor angle, angular rotation of recirculating balls and ball nut translation.*

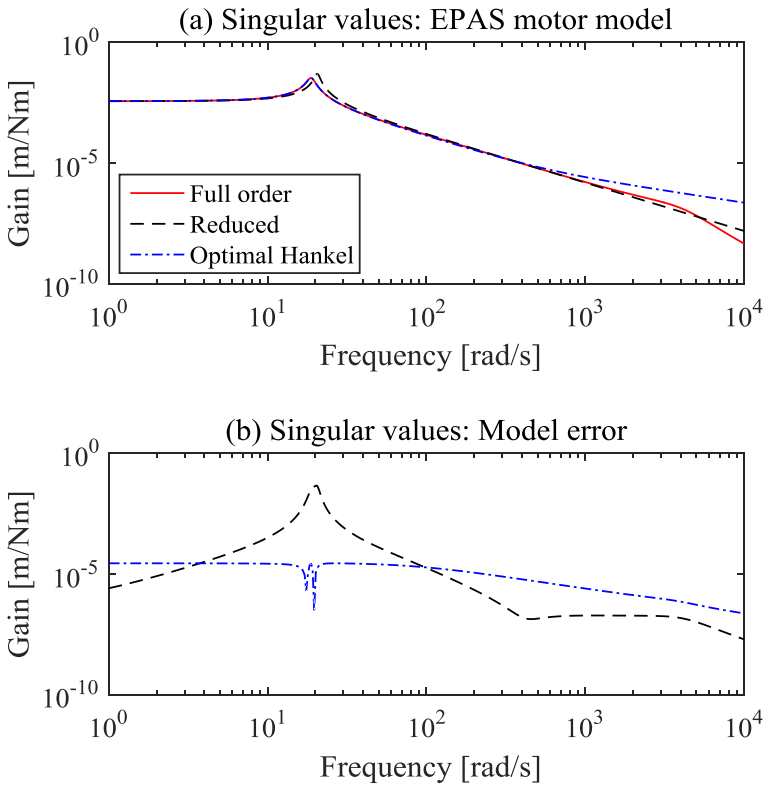

Figure 2.4: *(a) Singular values (frequency plot) of full order, reduced order and optimal Hankel EPAS motor model. (b) Singular values of the error system* $(\mathbf{G}(s) - \mathbf{G}_a(s))$ *for approximated models; reduced lower order and optimal Hankel.*

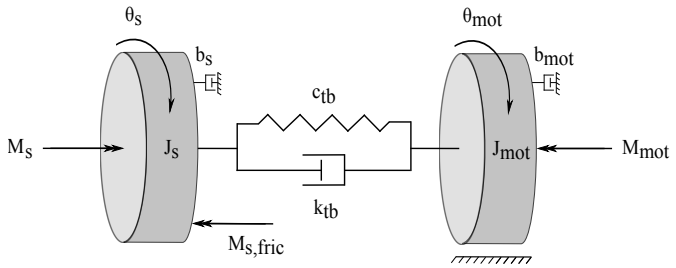

Figure 2.5: *Free body diagram of a steer-by-wire force-feedback system with 2-DOF; steering angle and motor angle.*

model error ($\mathbf{G}(s) - \mathbf{G}_a(s)$) singular values plot is shown in Fig. 2.4(b). For balanced residualization, the model order reduction holds if the error bound condition in Eq. (2.5) is satisfied, where n, k are actual and reduced number of states, and σ_i is *Hankel* singular value, see [41, pp. 459–478]. The infinity norm of the reduced model error is 0.047 at 20.27 rad/s. Thus satisfying the error norm upper bound criteria (= 0.068). Although one could use the optimal *Hankel* model because of lower error infinity norm, but we prefer our assumption for two reasons: (a) intuitive to realize stiff motor drive and (b) smaller error at lower frequencies for a good steady state performance.

$$||\mathbf{G}(s) - \mathbf{G}_a^k(s)||_\infty \leq 2 \sum_{i=k+1}^{n} \sigma_i \tag{2.5}$$

As a result, the effect of EPAS motor model can be included in the typical steering system (via rack to pinion transmission ratio) as shown in Fig. 2.2. This implies $J_{pin} = m_{eq,rack}/i_{rp}^2$, $b_{pin} = k_{eq,rack}/i_{rp}^2$ and $M_{mot,eff} = M_{mot} i_{mr}/i_{rp} = M_{mot} i_{mp}$. This model order reduction is considered in Paper A, Paper B and Paper D for the closed-loop control synthesis. However for the final simulation results, the derived controller is used with the full order model in IPG CarMaker.

2.1.2 Steer-by-wire force-feedback model

The inputs to the SbW-FFb system are steering torque (M_s) and motor torque (M_{mot}) from the FFb motor, refer Fig. 2.5. This hardware setup is relatively simpler compared to EPAS. The equations of motion are given in Eq. (2.6), with torsion bar torque as $M_{tb} = k_{tb}(\dot{\theta}_s - \dot{\theta}_{mot}) + c_{tb}(\theta_s - \theta_{mot})$. It should be noted that the direction of motor torque is considered opposite, as compared to EPAS, since it generates the complete steering feedback as resistance. Also, we have considered the case of direct motor to steering wheel coupling. In case there is a gear ratio for motor torque amplification, the effective motor impedance will also increase by the square of that gear ratio.

$$\begin{aligned} J_s\ddot{\theta}_s &= -b_s\dot{\theta}_s - k_{tb}(\dot{\theta}_s - \dot{\theta}_{mot}) - c_{tb}(\theta_s - \theta_{mot}) - M_{s,fric} + M_s \\ J_{mot}\ddot{\theta}_{mot} &= -b_{mot}\dot{\theta}_{mot} + k_{tb}(\dot{\theta}_s - \dot{\theta}_{mot}) + c_{tb}(\theta_s - \theta_{mot}) - M_{mot} \end{aligned} \tag{2.6}$$

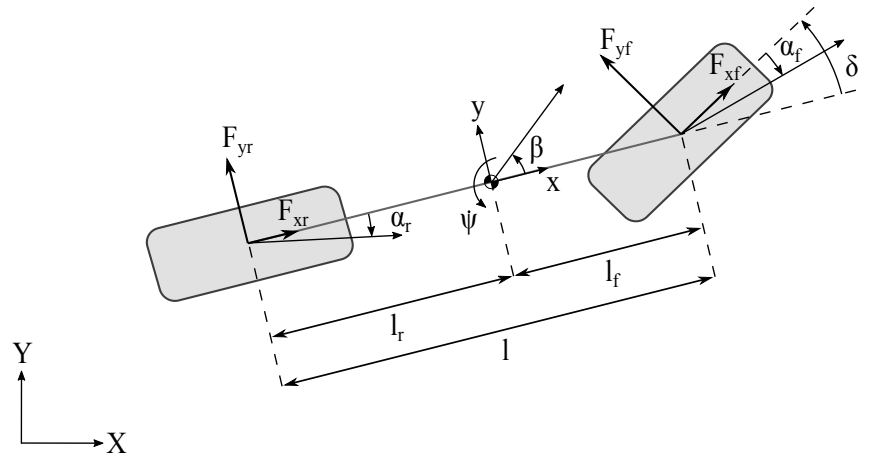

Figure 2.6: *Single track vehicle model in global coordinate system.*

2.2 Vehicle model

The single track vehicle model is used at first for our simplified analysis and controller development. The free body diagram in global coordinate system (XY) is shown in Fig. 2.6. It is a 3-DOF (degree of freedom) non-linear vehicle model with the following equations of motion (in vehicle frame or local coordinate system).

$$\begin{aligned} m\dot{v}_x &= F_{xf}\cos\delta - F_{yf}\sin\delta + F_{xr} + mv_y\dot{\psi} \\ m\dot{v}_y &= F_{xf}\sin\delta + F_{yf}\cos\delta + F_{yr} - mv_x\dot{\psi} \\ J_z\ddot{\psi} &= (F_{xf}\sin\delta + F_{yf}\cos\delta)l_f - F_{yr}l_r \end{aligned} \tag{2.7}$$

The lateral tire slip angle equations for front and rear axles can be derived as in Eq. (2.8). We have also included the front and rear axle tire relaxation time such that $T_{\alpha_i} = \sigma_{\alpha_i}/v_x$, where σ_{α_i} is corresponding relaxation length and i can be f or r for the respective axles. The body sideslip angle is defined as $\beta = \arctan(v_y/v_x)$.

$$\begin{aligned} \dot{\alpha_f} &= \frac{1}{T_{\alpha_f}}\left[\delta - \arctan\left(\frac{v_y + l_f\dot{\psi}}{v_x}\right) - \alpha_f\right] \\ \dot{\alpha_r} &= -\frac{1}{T_{\alpha_r}}\left[\arctan\left(\frac{v_y - l_r\dot{\psi}}{v_x}\right) + \alpha_r\right] \end{aligned} \tag{2.8}$$

A linearization is done around longitudinal velocity and neglecting the longitudinal dynamics. Then the controller is subsequently developed as a function of longitudinal velocity at different grid points. Assuming small road wheel and sideslip angles, and linear tire model ($F_{yi} = C_{\alpha_i}\alpha_i$), the state-space matrices become as follows with $\mathbf{x} = [v_y\ \dot{\psi}\ \alpha_f\ \alpha_r]^T$, $\mathbf{y} = F_{yf}$ and $\mathbf{u} = \delta$, where $\dot{\delta} = \dot{x}_{rack}i_{rp}/i_s$ and i_s is overall steering ratio

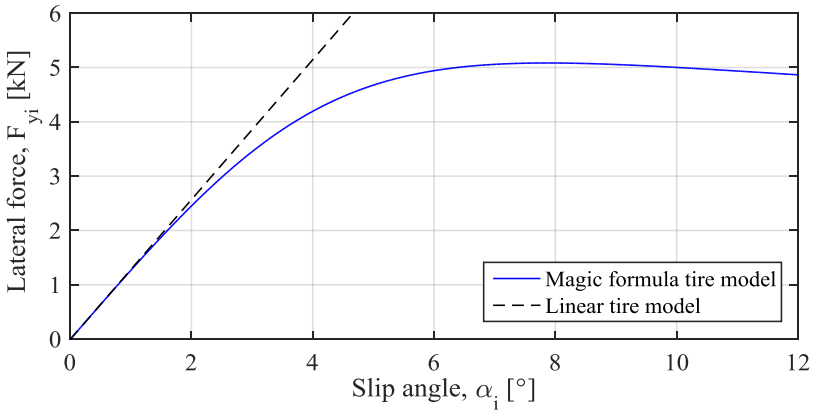

Figure 2.7: *Comparison of linear and non-linear (Magic formula) tire models under nominal load condition.*

(from pinion to road wheel angle).

$$\mathbf{A} = \begin{bmatrix} 0 & -v_x & \frac{C_{\alpha_f}}{m} & \frac{C_{\alpha_r}}{m} \\ 0 & 0 & \frac{C_{\alpha_f} l_f}{J_z} & \frac{-C_{\alpha_r} l_r}{J_z} \\ \frac{-1}{\sigma_{\alpha_f}} & \frac{-l_f}{\sigma_{\alpha_f}} & \frac{-v_x}{\sigma_{\alpha_f}} & 0 \\ \frac{-1}{\sigma_{\alpha_r}} & \frac{l_r}{\sigma_{\alpha_r}} & 0 & \frac{-v_x}{\sigma_{\alpha_r}} \end{bmatrix}, \ \mathbf{B} = \begin{bmatrix} 0 \\ 0 \\ \frac{v_x}{\sigma_{\alpha_f}} \\ 0 \end{bmatrix}, \mathbf{C} = \begin{bmatrix} 0 & 0 & C_{\alpha_f} & 0 \end{bmatrix} \text{ and } \mathbf{D} = 0 \quad (2.9)$$

The total steering moment (including the tire self-aligning moment) about the steer axis is given as a function of front axle lateral force (F_{yf}):

$$M_{steer} = F_{yf}(n_{tire} + n_{mech}) = F_{yf} n_{total} \quad (2.10)$$

where, n_{tire} is tire pneumatic trail and n_{mech} is caster trail. As a consequence, the resulting moment on the pinion is $M_{rack} = M_{steer}/i_s$. Eq. (2.10) is derived by taking the small angle approximation for kingpin and caster angles. The tire jacking force and scrub moment are neglected. This simplified model has been used in Paper B for the EPAS feedback control analysis and in Paper D for the steering feel reference model parameterization.

For EPAS validation purposes, it is done in CarMaker using a validated vehicle model. It has multiple DOF, apart from the already mentioned, such as load transfer, roll and pitch motions, wheel movements, etc. It also includes the non-linear '*Magic formula*' tire model. Since our focus is limited to lower slip angle range for a nominal tire-road surface condition, the linear tire model fulfills that purpose. Both the tire models are qualitatively compared in Fig. 2.7 on lateral force versus slip angle graph.

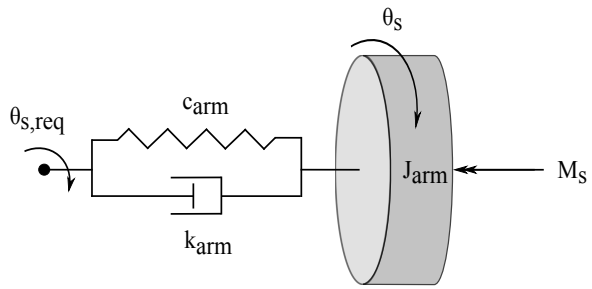

Figure 2.8: *Free body diagram of a simple muscular driver arm mechanical model as a 2^{nd} order system.*

2.3 Muscular driver arm model

The driver arm mechanics is required for the analytical comparison of the interaction dynamics between human and haptic controller. We have shown this in Paper B and Paper C for closed-loop EPAS and SbW-FFb respectively. Since we do not want to complicate the things unnecessarily, hence the simplest of the models has been presented. This model is used in the next chapter from performance, stability and robustness perspective of the closed-loop control.

$$\begin{aligned} J_{arm}\ddot{\theta}_s &= M_{arm} - M_s \\ M_{arm} &= k_{arm}(\dot{\theta}_{s,req} - \dot{\theta}_s) + c_{arm}(\theta_{s,req} - \theta_s) \end{aligned} \tag{2.11}$$

Here the driver arm is considered as a 2^{nd} order mechanical system, replicating the behavior of a typical PD (proportional-derivative) position control with an additional arm inertia. The free body diagram can be seen in Fig. 2.8. The equations of motion are given in Eq. (2.11). The steering angle request, $\theta_{s,req}$, can be assumed to be given by the neural path following control layer. The driver arm admittance (or impedance) parameters are time variant [30]. For a simplified analysis, we consider static values of the parameters as given in [11] for the worst case scenario of the haptic controller. For evasive maneuvers or high frequency steering inputs, the arms' muscle becomes highly stiff and rigidly coupled to the steering wheel. Hence, we consider the system input as driver arm torque (M_{arm}) for performance, stability and robustness analysis.

Chapter 3

Interaction between driver and steering

This chapter provides an overview on haptic feedback control methods, addressing the driver-vehicle interaction. The problem formulation covers shortcoming of existing open loop feedback control strategy. For proposed closed-loop possibilities, the feedback control content is based on Paper B and Paper C; whereas Paper D discusses on the reference generation. At last, the pros and cons of the closed-loop methods are also discussed along with the required potential improvements for future.

Before we present the state-of-the-art open loop control, we define some important test cases for our work regarding the evaluation of steering feedback. These cases are referred throughout the coming chapters for an understanding of the interaction dynamics. As shown in Fig. 3.1, a simplified driver-steering haptic interaction for an EPAS system. The torque (or force) and velocity exchange (power continuous) variables represent the natural realistic causality, obtained by combining the models from the previous chapter. The system inputs (as mentioned in 2.1) are driver torque, external motor torque (from vehicle motion control function) and external rack force (from the environment). Depending on the excitation source, the following test cases[1] are considered.

I. Driver excitation

II. External rack force excitation:
   (a) with driver-in-the-loop (or hands-on)
   (b) without driver-in-the-loop (or hands-off)

III. External motor torque (or vehicle motion control function) excitation:
   (a) with driver-in-the-loop (or hands-on)
   (b) without driver-in-the-loop (or hands-off)

[1]Case I and II are used in this chapter, whereas Case III will be further discussed in Chapter 4.

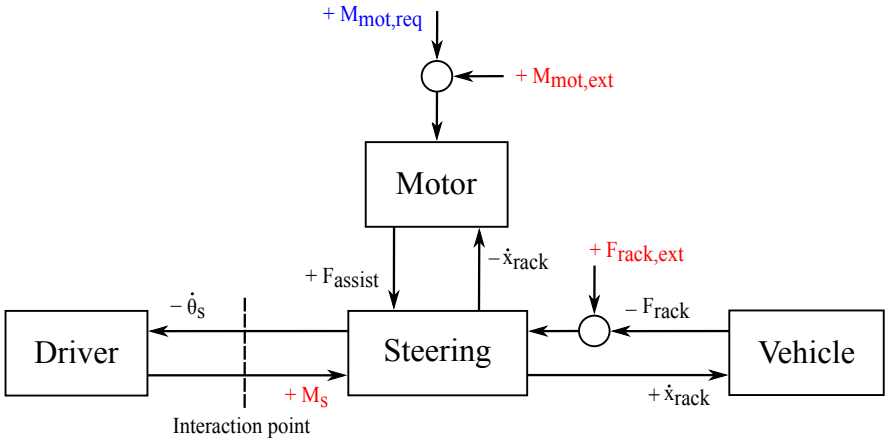

Figure 3.1: *A causal model of the haptic interaction between the driver and vehicle. The other driver feedback cues such as optical, acoustical, motion, etc. are excluded. The excitation sources are M_s, $F_{rack,ext}$ and $M_{mot,ext}$; and the steering feedback control input is $M_{mot,req}$.*

3.1 State-of-the-art: Open loop

In this thesis, we define the 'open loop control strategy' consisting of feedforward functions for steering feel; and no feedback control for reference tracking. A simplified control architecture is shown in Fig. 3.2. Depending on the steering system, either EPAS or SbW-FFb, the motor torque[2] is defined consequently. Because of its contribution for providing either a torque assistance or complete torque feedback to the driver respectively. Although this existing control strategy fulfills a broad spectrum of the desired steering feel requirements, but it lacks on a particular aspect of hardware impedance compensation. This is discussed further in detail.

3.1.1 Electric power assisted steering control

We will now consider EPAS system at first, and highlight its evolution from HPAS; and then discuss the SbW-FFb technology. A brief description on the 'open loop feedback control' steering feel functions is given as follows. The detailed information can be found in e.g. [9, 23, 28, 34].

(a) The basic assistance applies the motor torque as a function of torsion bar torque and vehicle speed. Typically the relation between them is non-linear, since this function is derived from HPAS. The modeling of HPAS system is not included here (refer [37] for more details). The origin of this non-linear behavior evolved from the steady state pressure difference in hydraulic chambers and torsion bar torque characteristic. The importance of this function can be understood, in a

[2]For SbW-FFb, θ_{mot} is equivalent to θ_{pin} in Fig. 3.2.

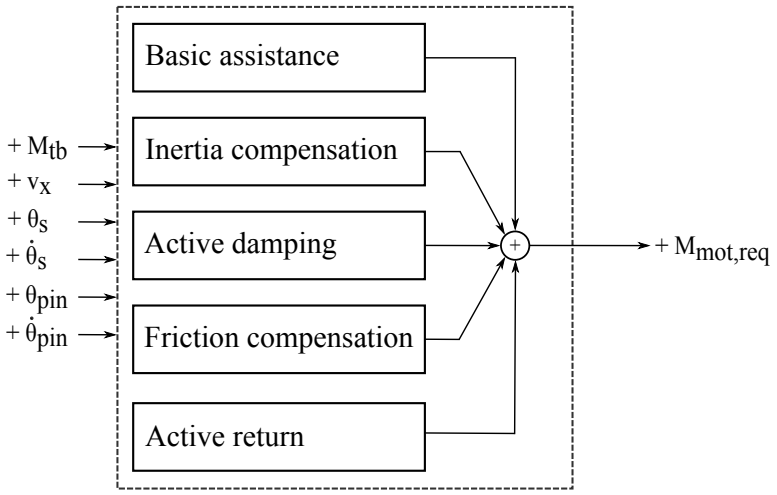

Figure 3.2: *Open loop steering feedback control strategy.*

quasi-static manner, as the desired steering effort to be applied for a given steering rack force from the vehicle.

(b) The inertia compensation functionality is added to overcome the effective motor impedance. This is a primary point of difference as compared to HPAS, since EPAS inherits huge steering rack impedance, caused by servo motor and its mechanical transmission ratio, as shown in Eq. (2.4). The motor torque component is computed using an estimated rotor (or pinion) acceleration. With this approach, it is difficult to compensate a higher percentage of additional impedance. Because the feedforward implementation has limitations due to model uncertainties [41]. Also, there are stability concerns due to noise amplification and time delay in the estimated acceleration signal as briefly explained in Paper A. A further detailed analysis on this particular aspect is discussed next as a part of the problem formulation.

(c) The inclusion of active damping, as the name suggests, manipulates the system viscous damping to avoid steering overshoot. This motor torque component is a function of pinion (or motor) angular velocity and vehicle speed. The considered assumption is that the motor to pinion mechanical connection is stiff, as shown in the previous chapter.

(d) The non-linear Coulomb friction on the steering rack is manipulated using friction compensation function. The goal is to achieve a desired on-center steering torque threshold. This motor torque component is primarily a function of pinion angular velocity.

(e) The active return function ensures a safe and desired steering wheel movement towards the on-center position, especially under free steer release situation. The

motor torque component is derived using the steering position/velocity control with a 'null' reference steering angle.

Consider a 2^{nd} order LTI model. The interaction dynamics with the model depends on its physical properties; inertia, damping and stiffness [27], which defines its frequency response. Coupling the passive system with a servo motor control results in an active response manipulation. It also results in a higher overall mechanical impedance due to servo motor [2, 13]. The effect is further amplified by the square of transmission ratio between the motor and system inertia, if any. As a consequence, the mechanical system response exhibits a low frequency low-pass filter characteristic in comparison to its passive setup due to higher effective system inertia.

The open loop steering feedback control (as shown in Fig. 3.2) is typically tuned to achieve a desired steering response under maximum periodic driver excitation (Case I) within 5 Hz [44]. However, the limitation of EPAS can be seen in Case II, where the pinion (or steering rack) acts as a mechanical low-pass filter for external road excitation [23]. This is due to the amplification of motor inertia by its mechanical transmission ratio, see the result of Section 2.1.1. Hence the effective pinion inertia increases massively, refer Paper A. Although the inertia compensation function mitigates this to some extent, but still it causes a loss of potentially useful (high frequency) external road feedback as compared to HPAS.

We will now explain this with some simulation results from the CarMaker environment. As it can be seen in Fig. 3.3(a), the frequency response function (FRF) of normalized external rack force to steering torque. The response gain is normalized with respect to its steady state gain for a better comparison at higher frequencies. The result is based on Case II(a) scenario, where the driver follows a straight line path despite of external disturbances (s.t. $\theta_{s,req} = 0$ rad in Eq. 2.11). In this case, the driver arm muscles can be assumed as highly tensed. The passive EPAS iteration is the inclusion of motor hardware dynamics without any torque support, $M_{mot} = 0$ Nm. With the current open loop control, the system bandwidth[3] ($\approxeq$ 3.5 Hz) is although similar with passive EPAS but the steering torque response is less attenuated at higher frequencies. Primarily this is due to the inertia compensation function. To further emphasize our point on the effect of system inertia, an additional (hypothetical) iteration exhibits the improvement in system bandwidth ($\approxeq$ 9.5 Hz) for passive EPAS with reduced motor inertia in Fig. 3.3(a). A similar conclusion can be drawn from Fig. 3.3(b), where the FRF of normalized external rack force to rack displacement is shown for Case II(b) scenario, s.t. $M_s = 0$ Nm. Therefore, the lower effective system inertia results in a reduced filtering of external road feedback on steering torque and rack displacement.

Since the above results are difficult to replicate on an actual vehicle, we performed experiments on the steering test rig to verify the simulation findings. On the rig, the steering rack is mechanically connected to two separate actuators. One of them simulates a pre-selected spring and damping characteristic (attributing to F_{rack}); and

[3]Bandwidth corresponds to the frequency at which the absolute gain drops by 3 dB or 29.21%.

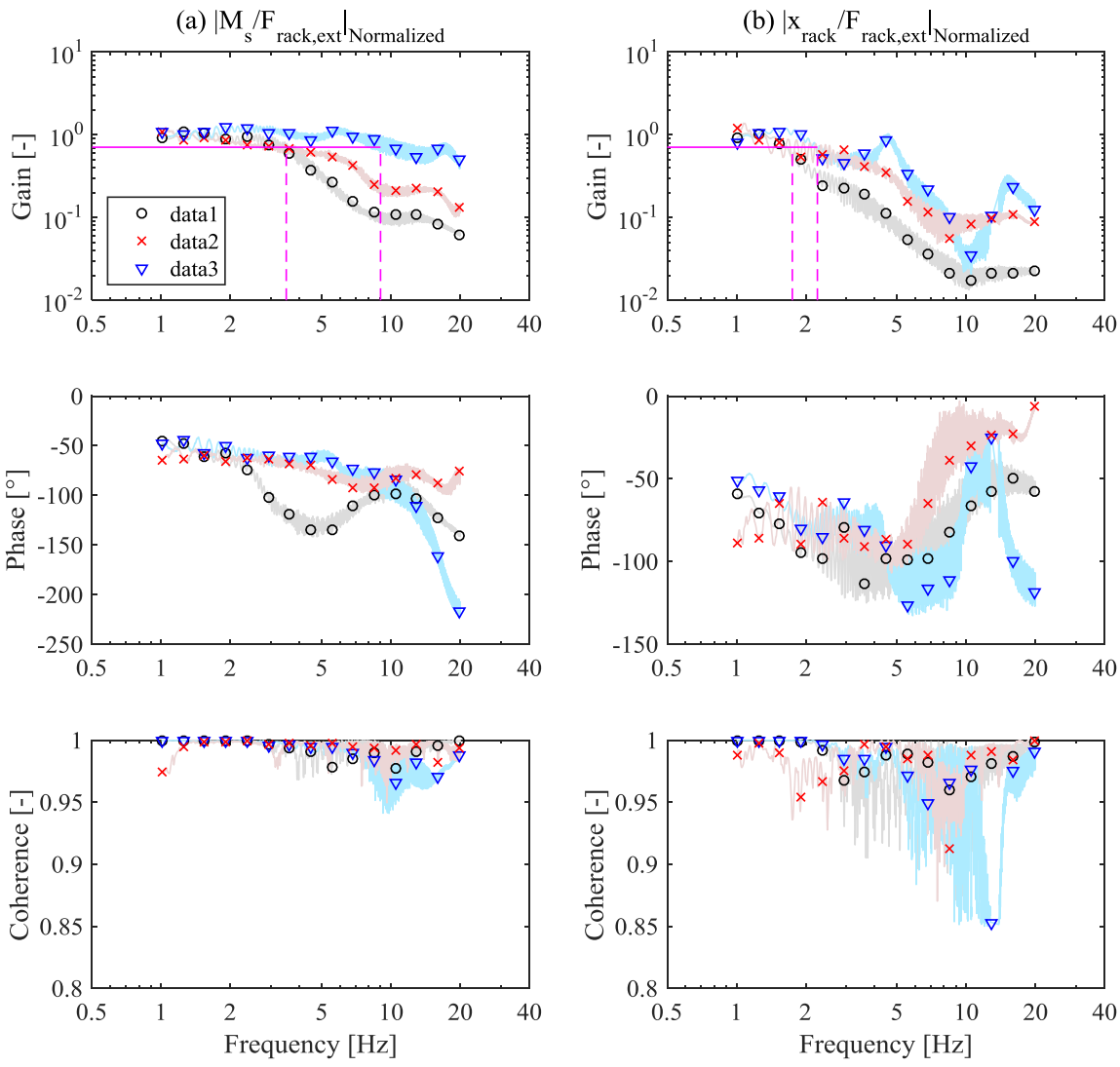

Figure 3.3: *Post-processed EPAS simulation result of normalized external steering rack force to (a) steering torque and (b) rack displacement frequency response at 75 km/h vehicle speed. The normalization has been done with respect to its steady state gain. The plot details are: data1 – passive system, data2 – open loop control and data3 – modified passive system with lower motor inertia. The 'magenta' colored --- lines indicate the corresponding system bandwidth.*

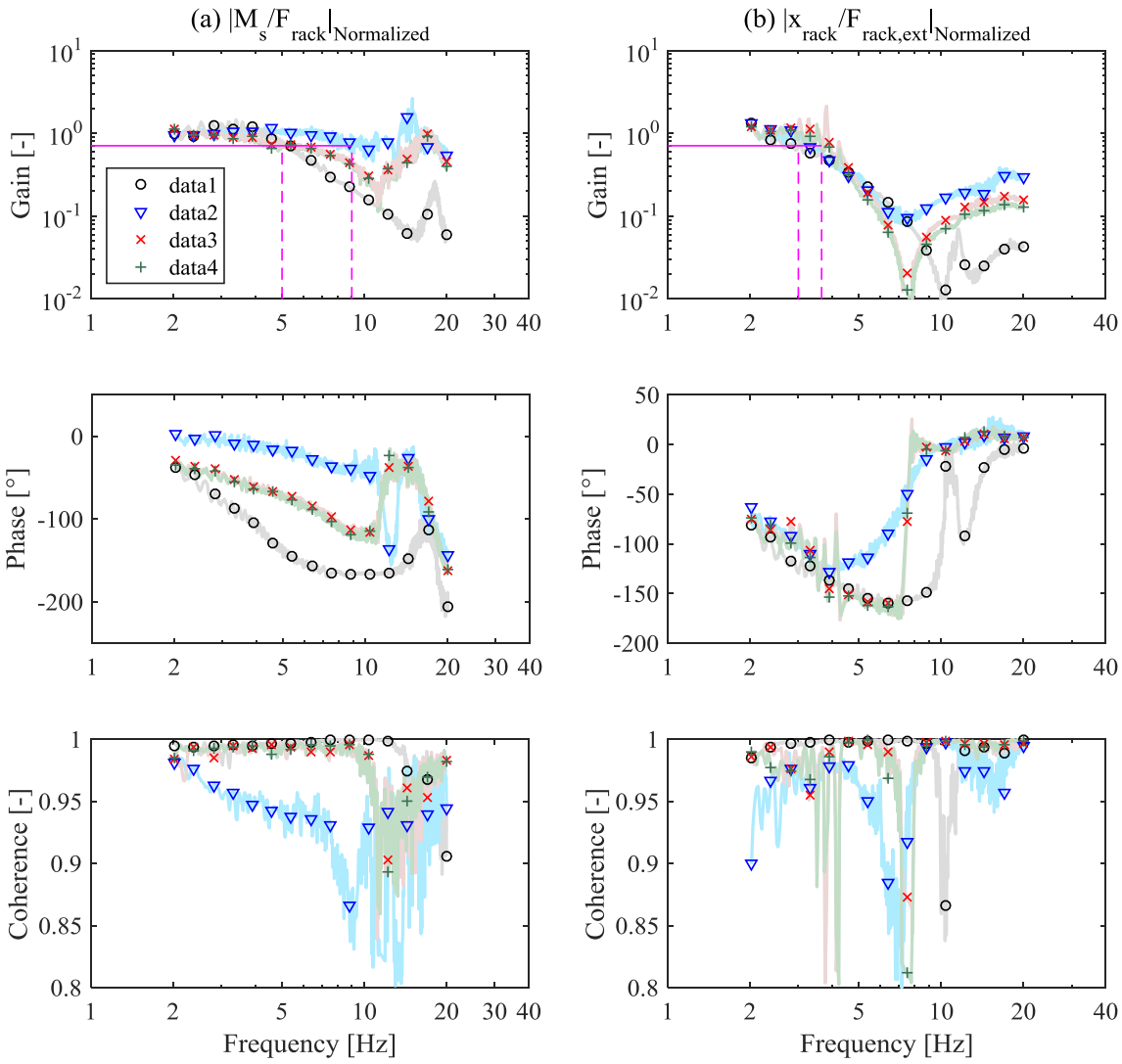

Figure 3.4: *Post-processed EPAS test rig result of normalized external steering rack force to (a) steering torque and (b) rack displacement frequency response at different vehicle speeds. The normalization has been done with respect to its steady state gain. The plot details are: data1 – passive system at 0 km/h, data2, data3 and data 4 – open loop control at 0 km/h, 75 km/h and 90 km/h respectively. The 'magenta' colored --- lines indicate the corresponding system bandwidth.*

the external rack force disturbance is created by the other actuator. Refer Fig. 3.4, the frequency response of normalized external rack force to steering torque and rack displacement for fixed and freely rotating steering wheel, thus simulating Case II(a) and (b) respectively. In passive EPAS condition for Case II(a), the system bandwidth is approx. 5 Hz as shown in Fig. 3.4(a). With the active steering feedback control, the system bandwidth increases to 9 Hz at 0 km/h vehicle speed. This is because of the inertia compensation function. Its effect is reduced at higher vehicle speeds, since the system bandwidth drops to approx. 5 Hz for both 75 km/h and 90 km/h cases. However, the key takeaway is that with open loop EPAS control, high frequency steering torque response is less attenuated as compared to the passive condition. A similar behavior can be observed in rack displacement response, see Fig. 3.4(b), under free steering wheel rotation. Thus the test rig measurements qualitatively confirm the simulation finding. For skilled test drivers, the relevant steering feedback requirement is usually defined in the range of $20-30$ Hz [23]. Keeping this as criteria, the performance of the open loop control (in terms of external rack force to steering torque FRF) is quite limited. Based on these observations, we raise two questions.

(a) Is it possible to improve the steering feedback response by closed-loop control?

(b) What are the challenges involved in closed-loop control compared to open loop approach?

3.1.2 Force-feedback control

The open loop FFb architecture is a straightforward solution and readily used, see e.g. [5, 19, 24]. Using different signals such as angular position and velocity, the motor torque reference is computed as shown in Fig. 3.2. However due to additional servo motor impedance, the actual torque is compromised. Furthermore, the external steering rack forces need to be estimated and then adapted for a desired road feedback.

For a simple reasoning, we objectify the SbW-FFb performance (from the test rig) using Case I. The reference motor torque is assumed as a function of angular position for a virtual steering feedback. The FRF of measured torque to feedback motor angular position and velocity are shown in Fig. 3.5(a) and (b) respectively. The high frequency reference tracking (> 2 Hz) is deteriorated because of FFb motor impedance. As a result, the reference torque deviates from the measured torque in Fig. 3.5(c). Even if the reference would have contained the external road feedback information, these results would have shown a similar behavior within this frequency range. An ideal SbW-FFb hardware setup demands a reasonable system bandwidth to meet the given steering feedback requirement. With the observations above, we can formulate two questions.

(a) Would it be possible to improve the performance of open loop control by using closed loop methods?

(b) How to make an objective comparison between the different control methods?

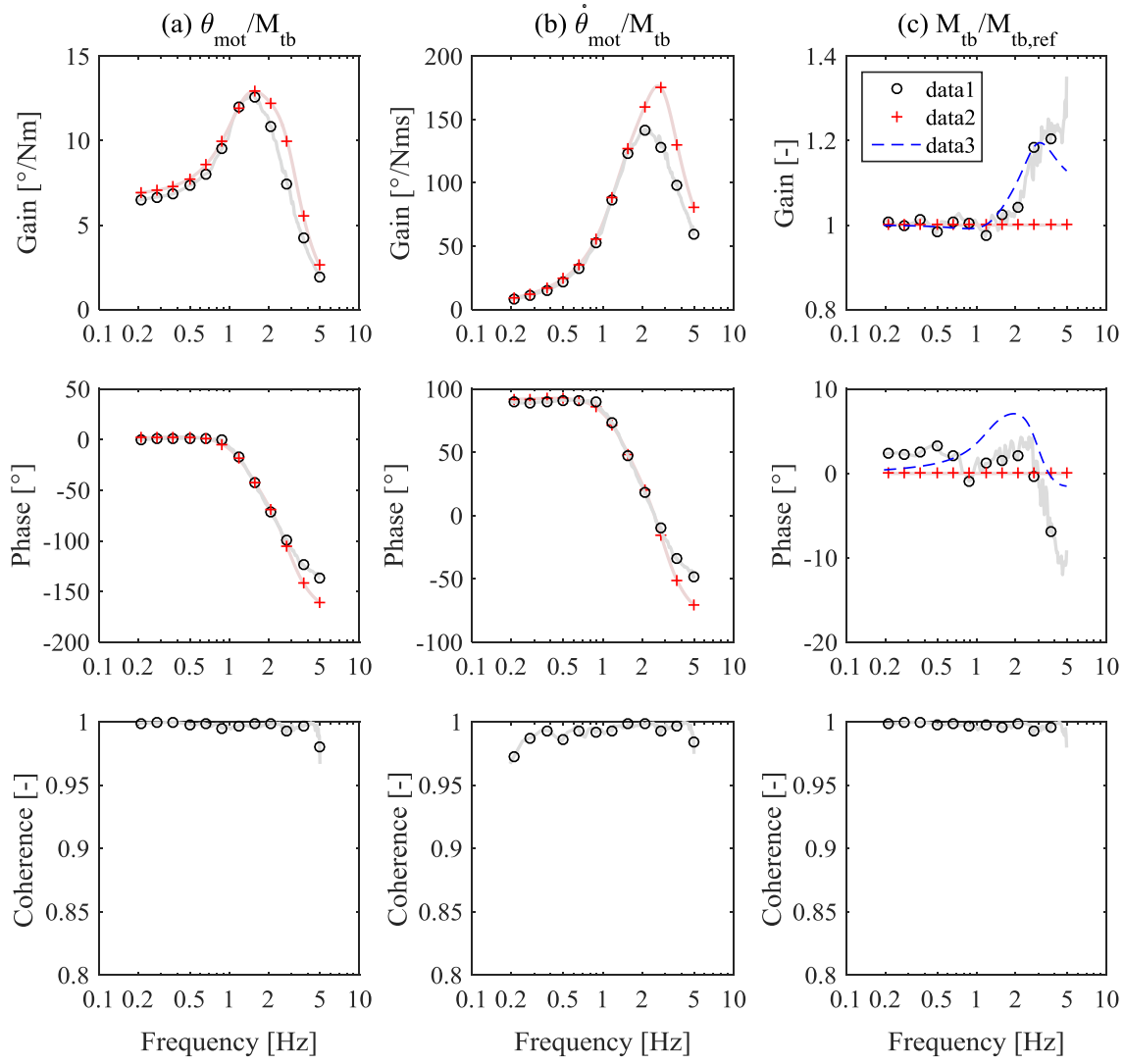

Figure 3.5: *Post-processed SbW-FFb test rig result of torsion bar torque to (a) motor angular position and (b) angular velocity and (c) reference to actual torsion bar torque frequency response. The plot details are: data1 – open loop control, data2 – reference (at 75 km/h vehicle speed) and data3 – derived analytical function using Eq.* (2.6).

3.2 Introduction to Closed-loop

We define the term 'closed-loop' for control strategies where the tracking of a given signal is performed. From control theory, the two primary concepts are; impedance and admittance control. The 'impedance control' is also known as torque (or force) control. Position control is a common terminology for 'admittance control'. In the context of the steering system, the potential advantages of the closed-loop control are as follows.

(a) Hardware independent steering feedback response can be achieved, such that the higher level control (or reference) would be 'portable' to different environments (for example driving simulator and hardware-in-the-loop test rig), other closed-loop vehicle steering systems, etc.

(b) Relatively simpler and more intuitive tuning of the higher level control based on the steering feedback requirements.

(c) Independent lower level control tuning for a defined tracking performance as the objective.

3.2.1 Impedance and Admittance control

A typical closed-loop haptic feedback control configuration consists of two loops; inner and outer as shown in Fig. 3.6, refer [2, 18, 36, 40] for more details. The presented layout in Fig. 3.6 is only valid for a single port human interaction with system coupled to an actuator. The outer-loop is responsible for the reference generation and the inner-loop for the reference tracking (of the outer-loop). The two single-input single-output possibilities are impedance and admittance control. They both require measured torque and angular position signals. They are complimentary to each other because one signal is used to generate the reference and the other signal is tracked.

In Laplace domain, the impedance is defined as the transfer function between torque and angular velocity in power-continuous coupling. For our work, we simplify that to torque to angular displacement in terms of virtual work done [27]. For admittance it is vice versa, i.e. the transfer function between angular displacement to torque. In impedance control, the outer-loop generates the reference torque by using the measured angular position and 'virtual impedance'. On the contrary, the measured torque generates the reference angular position via the 'virtual admittance' in admittance control.

There are examples in the literature of both the approaches being addressed, but not compared to each other. Such examples are, [17, 21, 28] for EPAS and [4, 19, 22, 24, 48] for SbW-FFb. This thesis makes an investigation on the conceptual differences between the two control approaches. An objective comparison between impedance and admittance control is presented in Paper B and Paper C for EPAS and SbW-FFb systems respectively. These concepts are applied at the torsion bar, for signals torsion bar torque and (pinion or FFb motor) angular position, and not at the steering wheel. The motive of this choice is provided in Paper D.

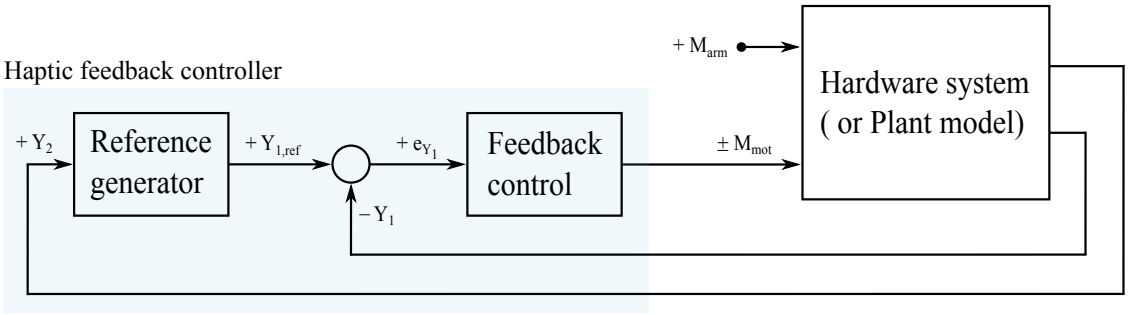

Figure 3.6: *Closed-loop haptic feedback control layout for a typical steering hardware system.*

Stability can be studied from uncoupled and coupled perspective. The uncoupled stability defines the systems' isolated behavior; whereas the stability of the haptic feedback controller with human interaction is termed as coupled stability. Uncoupled stability can be derived in two steps. Firstly, checking stability for the inner-loop in isolation such that the servo control loop (or closed-loop plant) is stable independent of the reference. In the second step, there are two ways to derive overall stability; (a) how much faster[4] reference dynamics one could realize on the outer-loop, given a certain closed-loop plant behavior or (b) to define an additional criteria for the inner-loop, given the reference dynamics in the outer-loop. The last step is to verify the coupled stability, because to consider the situation with driver-in-the-loop. It should be noted that uncoupled stability in itself does not guarantee coupled stability [13]. Coupled instability is a well known phenomenon, particularly in admittance control, also known as contact instability [10]. It could occur for high driver arm impedance. Therefore with a limited closed-loop plant performance, there is always an upper bound on how fast the reference dynamics in the outer-loop can be realized. The linear impedance and admittance control laws, for our purpose, are formulated by abiding these criteria.

3.2.2 Coupled stability analysis

Linear system theory is used for coupled stability analysis. We treat the EPAS and SbW-FFb case in a common analysis framework due to their similarities. For suitability, the Laplace transform of the LTI plant can be written as follows with $\mathbf{y} = [\theta_s \ \theta_k \ M_{tb}]^T$ and $\mathbf{u} = [M_{arm} \ M_{mot}]^T$, where k = $\{pin$ or $mot\}$ for EPAS and SbW-FFB respectively.

$$\begin{aligned} \mathbf{G}(s) &= \mathbf{C}(s\mathbf{I} - \mathbf{A})^{-1}\mathbf{B} + \mathbf{D} \\ \text{where, } G_{22} &= \theta_k(s)/M_{mot}(s) \\ G_{32} &= M_{tb}(s)/M_{mot}(s) \end{aligned} \tag{3.1}$$

[4]Faster dynamics means either higher stiffness in impedance or lower inertia in admittance reference respectively.

The resulting loop gain with their respective control laws become as Eq. (3.2). The impedance and admittance feedback control transfer functions are $H_{fb,M}$ and $H_{fb,\theta}$. Their respective reference transfer functions are $H_{ref,M}$ and $H_{ref,\theta}$. These loop gains appear in both uncoupled and coupled stability.

$$L_i = \begin{cases} H_{fb,M}(G_{32} - H_{ref,M}G_{22}) & i = M \text{ for impedance control} \\ H_{fb,\theta}(G_{22} - H_{ref,\theta}G_{32}) & i = \theta \text{ for admittance control} \end{cases} \tag{3.2}$$

Linear impedance control design

A simple proportional-integral (PI) torque feedback control is sufficient to meet the desired objectives of (a) impedance compensation and (b) reference tracking. The control law is given in Eq (3.3). The negative motor torque is for EPAS (because M_{tb} and M_{mot} act in the same direction) and vice versa for SbW-FFb. But both represent negative (torque) feedback. The effective pinion torque assist in EPAS is $M_{mot,eff} = M_{mot}i_{mp}$, where i_{mp} is the motor to pinion transmission ratio. This ratio is possible for SbW-FFb systems also with an indirect coupling, but we consider a direct FFb-motor coupling to the steering wheel such that $i_{mp} = 1$.

$$M_{mot} = \mp\big(\alpha_1 e_M + \alpha_0 \int_0^t e_M d\tau\big), \text{where } e_M = M_{tb,ref} - M_{tb} \tag{3.3}$$

With the proportional torque feedback, the mechanical impedance is reduced by a factor $(1 + \alpha_1 i_{mp})$, see e.g. [12, 27], Paper B and Paper C. Whereas the integral part ensures a lower steady state tracking error and disturbance rejection. Although both the gains should be higher, Eq. (3.4) is a necessary and sufficient condition. For the given expression and the type of steering system, $\alpha_1' = 1 + \alpha_1 i_{mp}$ and $c_{mot} = 0$ Nm/rad. The expression is derived for the feedback (or servo) control loop with $H_{ref,M} = 0$ and neglecting the smaller terms (w.r.t. a stiff torsion bar). The constraint ensures closed-loop left half plane (LHP) poles, assuming no right half plane (RHP) pole-zero cancellation. The graphical representation of this inequality between α_1-α_0 for EPAS and SbW-FFb are shown in Fig. 3.7(a) and Fig. 3.8(a) respectively.

$$\alpha_0 < \frac{1}{i_{mp}}\left[\left(\alpha_1' + \frac{J_k}{J_s + J_{arm}}\right)^2 \frac{k_{tb}}{J_k} + \alpha_1' \frac{b_k}{J_k} + \frac{J_k b_s}{(J_s + J_{arm})^2} + (\alpha_1' k_{tb} + b_k)\frac{c_k}{c_{tb} J_k}\right] \tag{3.4}$$

The key interpretation from these figures is '*for a selected phase margin*[5] *(ϕ_m), it is possible to increase the feedback control gains and its bandwidth (f_{in}) simultaneously*'. In reality, the gains are limited by the maximum actuator capability. In the next step, we check the closed-loop sensitivity against the parameter variation. The effect on performance and stability as a function of J_{arm} and v_x is presented in Fig. 3.7(b) and (c) respectively for EPAS. Whereas the effect of J_{arm} variation on SbW-FFb is shown

[5]It is a direct measure against the time delay uncertainty, refer [41] for details.

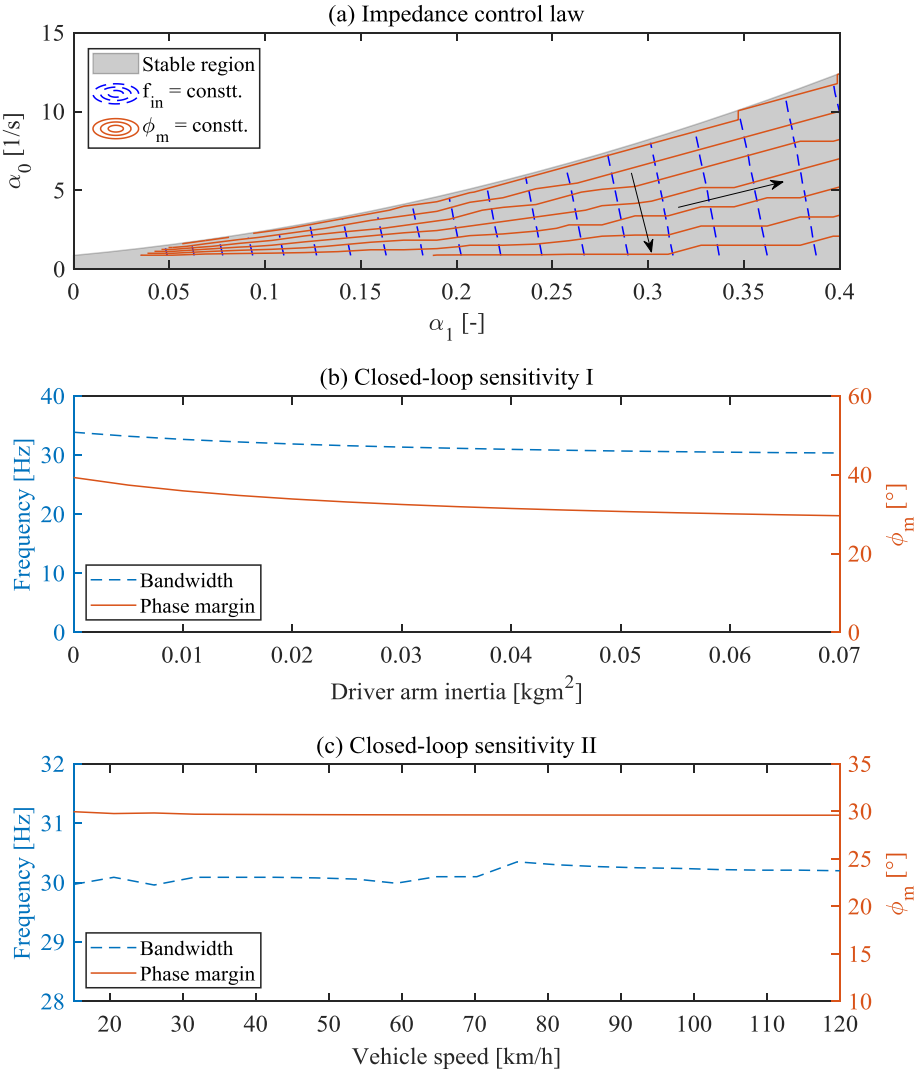

Figure 3.7: *EPAS impedance control design results. (a) Stability constraint between the feedback control gains α_1-α_0 from Eq.* (3.4)*. The 'blue' colored --- lines represent constant bandwidth (f_{in}) and the 'orange' colored — lines represent constant phase margin (ϕ_m). The arrows indicate the direction of increasing f_{in} and ϕ_m. (b) Closed-loop sensitivity of driver arm inertia on f_{in} and ϕ_m. (c) Closed-loop sensitivity of vehicle speed on f_{in} and ϕ_m.*

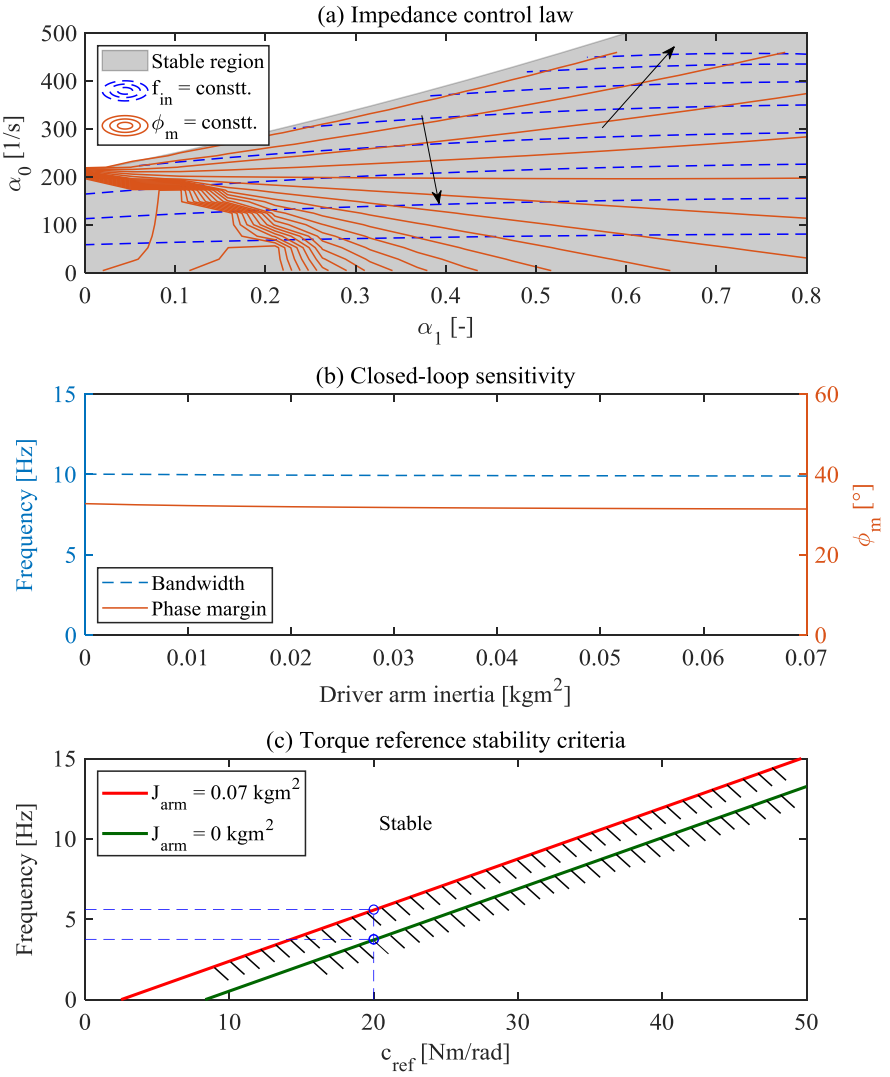

Figure 3.8: *SbW-FFb impedance control design results. (a) Stability constraint between the feedback control gains α_1-α_0 from Eq. (3.4). The 'blue' colored --- lines represent constant bandwidth (f_{in}) and the 'orange' colored — lines represent constant phase margin (ϕ_m). The arrows indicate the direction of increasing f_{in} and ϕ_m. (b) Closed-loop sensitivity of driver arm inertia on f_{in} and ϕ_m. (c) The stability criteria in Eq. (3.8) between impedance reference stiffness and inner-loop bandwidth for different driver arm inertia. The unstable regions are hatched for convenience.*

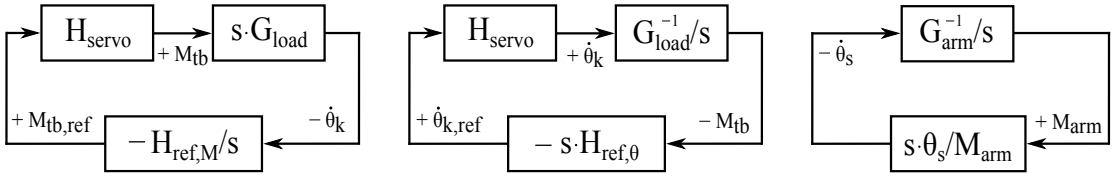

(a) Impedance control loop (b) Admittance control loop (c) Driving port admittance loop

Figure 3.9: *Closed-loop feedback interconnection for uncoupled and coupled stability analysis using the power-continuous variables. (a) Impedance and (b) Admittance control loop gains with $G_{load} = G_{22}/G_{32}$. (c) Interaction port driving admittance loop gain.*

in Fig. 3.8(b). The results show that the impedance control is robust enough against these parameters' variation because both the bandwidth and inner-loop phase margin do not vary significantly.

Taking a step further in analyzing the uncoupled stability, such that the system is stable in isolation. Considering the outer-loop (stated to be an impedance) with $H_{ref,M} = J_{ref}s^2 + b_{ref}s + c_{ref}$, the closed-loop plant is constrained to have an admittance causality. The stability criteria can be derived for the two possibilities. At first given a predefined servo control bandwidth (ω_{in}), we try to find the reference stiffness bound (if any, with reasonable assumptions $J_{ref} = 0$ kgm^2, $b_{ref} = 0$ Nms/rad and $k_{tb} \to 0$ Nms/rad). The resulting (simplified) loop gain, see Fig. 3.9(a), is given below.

$$L_M = -H_{ref,M}H_{servo}\frac{G_{22}}{G_{32}} = c_{ref}\left(\frac{1}{1+(1/\omega_{in})s}\right)\left(\frac{1}{(J_s+J_{arm})s^2+b_s s}+\frac{1}{c_{tb}}\right) \tag{3.5}$$

$$c_{ref}^2 + c_{tb}\left(2+\frac{b_s}{\omega_{in}(J_s+J_{arm})}-\frac{c_{tb}}{\omega_{in}b_s}\right)c_{ref} + c_{tb}^2\left(1+\frac{b_s}{\omega_{in}(J_s+J_{arm})}\right) > 0 \tag{3.6}$$

For a necessary and sufficient stability condition, the quadratic constraint (with non-negative solution) in Eq. (3.6) can provide an upper bound on c_{ref}. This explains how much maximum stiffness we could achieve in the outer-loop given a certain inner-loop characteristic. And if the servo bandwidth satisfies $\omega_{in} > \big(c_{tb} - b_s^2/(J_s+J_{arm})\big)^2/(4b_s c_{tb})$, then the stability is maintained at all times irrespective of c_{ref}. Graphically, it can be seen in Fig. 3.10(a) for EPAS system. On the contrary for a given c_{ref}, the inner-loop can be designed using Eq. (3.7) to ensure that it is stable $\forall\ c_{ref} \geq 0$ Nm/rad. As a result, the stable region in Fig. 3.10(b) has shrunk in comparison to Eq. (3.4) and Fig. 3.7(a). Similarly for SbW-FFb, the sufficient stability condition in Eq. (3.8) has been derived using the Nyquist criterion (with the same assumptions as above and $c_{tb} \to \infty$ Nm/rad). The expression emphasizes that with increasing J_{arm}, the minimum bandwidth requirement also increases for a pre-determined c_{ref}, refer Fig. 3.8(c).

$$\alpha_0 < \alpha_1\big(b_k + \alpha_1' k_{tb}\big)/J_k \tag{3.7}$$

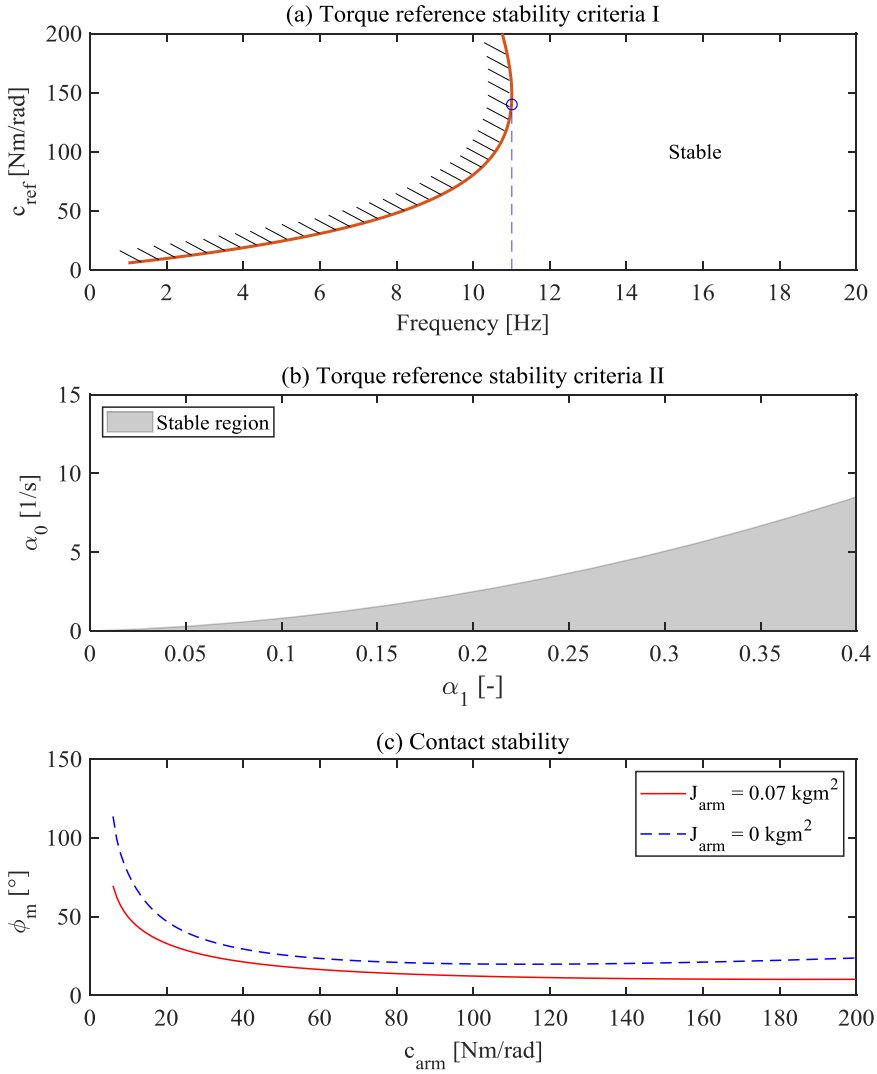

Figure 3.10: *EPAS impedance control design results. (a) The stability criteria in Eq.* (3.6) *between inner-loop bandwidth and impedance reference stiffness. The unstable region is hatched for convenience. (b) The stability criteria in Eq.* (3.7) *between the feedback control gains* α_1-α_0. *(c) The driving port admittance loop gain phase margin (robustness measure of contact stability) as a function of drivers' arm stiffness for different arm inertia.*

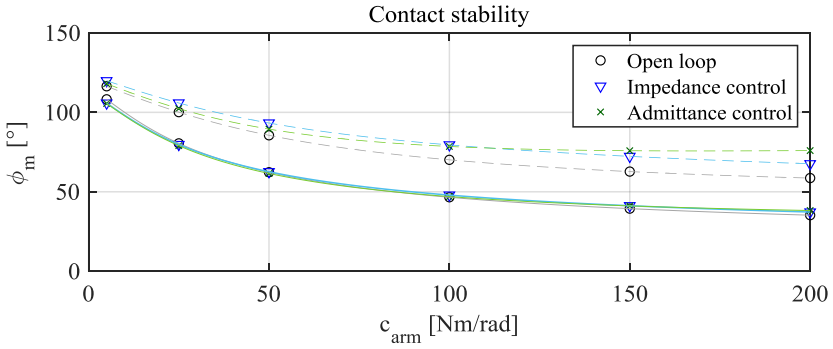

Figure 3.11: *SbW-FFb driving port admittance loop gain phase margin as a function of drivers' arm stiffness. The figure shows ϕ_m variation for open loop, impedance and admittance control for $J_{arm} = 0$ kgm^2 (---) and $J_{arm} = 0.07$ kgm^2 (—) respectively.*

$$\omega_{in} > (c_{ref}/b_s - b_s/(J_s + J_{arm})) \tag{3.8}$$

The reference impedance also consists of J_{ref} and b_{ref} parameters, but with suitable assumptions it can be proven that they would not affect the stability as a sufficient condition. However, we could only realize a proper and real-time implementable (or causal) impedance reference. Therefore, it needs some kind of filtering and estimation for angular acceleration (and also angular velocity if not available explicitly). For this purpose, a second-order low pass filter, $H_{lp}(s)$, is used with a desired filter time constant 4.5 ms) and damping ratio (0.707).

Once the uncoupled stability is ensured, then the coupled stability depends on the single-port interaction point driving admittance defined in terms of $Z(s) = s\theta_s/M_{arm}$. The controller parameters are defined to achieve a passive driving admittance, thus fulfilling the conditions of a positive real function: no RHP poles, no simple poles and $\mathrm{Re}[Z(j\omega)] \geq 0$, $\forall\ \omega \in \mathbb{R}$, refer [31] for the definition. This is a necessary and sufficient stability condition for the driving admittance when coupled to an arbitrary passive environment [13]. Although the conclusion is similar to passivity theorem, see [31], which states 'the feedback connection of two passive systems is passive', but the above condition is not sufficient to guarantee asymptotic stability as explained in [14]. Since in our case the environment represents the driver interaction and we assume a '*strictly*' passive drivers' muscular arm impedance as $G_{arm}^{-1}(s)/s = k_{arm} + c_{arm}/s$. Then the coupled system is asymptotically stable as described in [27], because this condition holds if one system is passive and the other as strictly passive. Hence, the coupled (or contact) stability is maintained at all times. The resulting loop gain, refer Fig. 3.9(c), is $L_d = G_{arm}^{-1}(\theta_s/M_{arm})$. The loop gain phase margin variation as a function of the arm stiffness is shown in Fig. 3.10(c) and Fig. 3.11 for the two steering systems respectively.

An interesting behavior can be observed for EPAS, where the plant model driving port admittance is not passive (as the Nyquist contour of $Z(s)$ crosses the open RHP or the phase exceeds $+90°$). This is due to a RHP zero in body sideslip response at higher

vehicle speeds. As a consequence, driving port admittance passivity is lost. Because the steering stiffness is a function of rack force (which subsequently depends on the front axle slip angle). If the feedback control is designed sensibly, then the closed-loop driving port admittance can be guaranteed to retain passivity as described above.

Linear admittance control design

The admittance control law is derived using the previously mentioned impedance control function. We equate the respective loop gains (or characteristic equations), such that $L_\theta = L_M$, to obtain a sufficient admittance control law. The result is given in Eq. (3.9) with a reasonable assumption $H_{ref,M}H_{ref,\theta} = 1$. This condition holds because the outer-loop represents an admittance causality (inverse of impedance reference).

$$L_M \overset{!}{=} L_\theta \implies H_{fb,\theta} = -H_{fb,M}H_{ref,M} \tag{3.9}$$

The relationship is simplified using $H_{fb,M} = \mp(\alpha_1 + \alpha_0/s)$ and $H_{ref,M} = J_{ref}s^2 + b_{ref}s + c_{ref}$. In general, the inner-loop minimizes the error in angular position (and its integral), velocity and acceleration for tracking an admittance reference. Eq. (3.10) defines the motor torque. The positive sign is for EPAS and vice versa for SbW-FFb, although both apply the negative angular position feedback. The purpose of β_3, β_2 and β_1 is to manipulate the system inertia, damping and stiffness respectively for (a) impedance compensation; and β_0 for (b) reference tracking, see Paper B and Paper C for details.

$$M_{mot} = \pm\big(\beta_3\ddot{e}_\theta + \beta_2\dot{e}_\theta + \beta_1 e_\theta + \beta_0\int_0^t e_\theta d\tau\big), \text{where } e_\theta = \theta_{k,ref} - \theta_k \tag{3.10}$$

There are two ways to tackle the system inertia; either assuming $\ddot{\theta}_{k,ref} = 0$ rad/s^2 and using $\mp\beta_3\ddot{\theta}_k$ for inertia compensation (such that $\beta_3 < 0$) or use the complete control law as above with $\beta_3 > 0$ for a desired reference tracking. The first method is a typical feedforward inertia compensation as in open loop control; whereas the second method should be realized to follow the reference, only with $\beta_3 > 0$ for a minimum phase system. Furthermore, a real-time implementable (and causal) admittance feedback control is only possible with filtering and estimation for angular acceleration and velocity errors. For this, the same second-order low pass filter as in impedance reference is implemented.

Eq. (3.11) is a necessary and sufficient condition for the inner-loop stability such that $H_{ref,\theta} = 0$ and assuming $c_{tb} \to \infty$ Nm/rad. This constraint ensures closed-loop LHP poles (with no RHP pole-zero cancellation) and no loop gain encirclement of -1. The graphical representation of the inequality relation between β_3-β_0 (given β_1 and β_2) for EPAS and SbW-FFb are shown in Fig. 3.12(a) and Fig. 3.13(a) respectively. These two parameters are chosen because they are responsible for inertia compensation and reference tracking respectively. β_1 and β_2 are pre-selected for a desired performance as explained in Paper B and Paper C, and the aim is to improve the feedback control by exploiting β_3. The conclusion from these figures are, (a) '*for a selected phase margin*

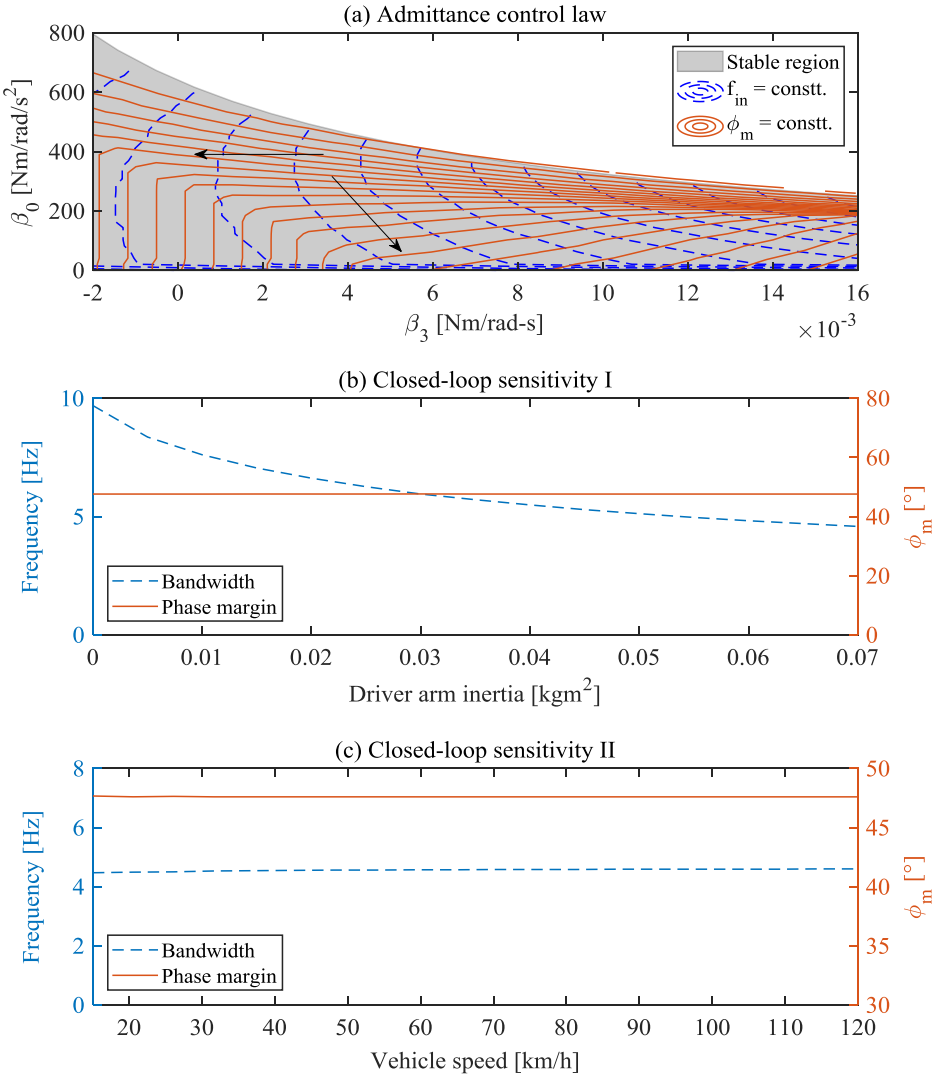

Figure 3.12: *EPAS admittance control design results. (a) Stability constraint between the feedback control gains β_0-β_3 from Eq.* (3.11)*. The 'blue' colored --- lines represent constant bandwidth (f_{in}) and the 'orange' colored — lines represent constant phase margin (ϕ_m). The arrows indicate the direction of increasing f_{in} and ϕ_m. (b) Closed-loop sensitivity of driver arm inertia on f_{in} and ϕ_m. (c) Closed-loop sensitivity of vehicle speed on f_{in} and ϕ_m.*

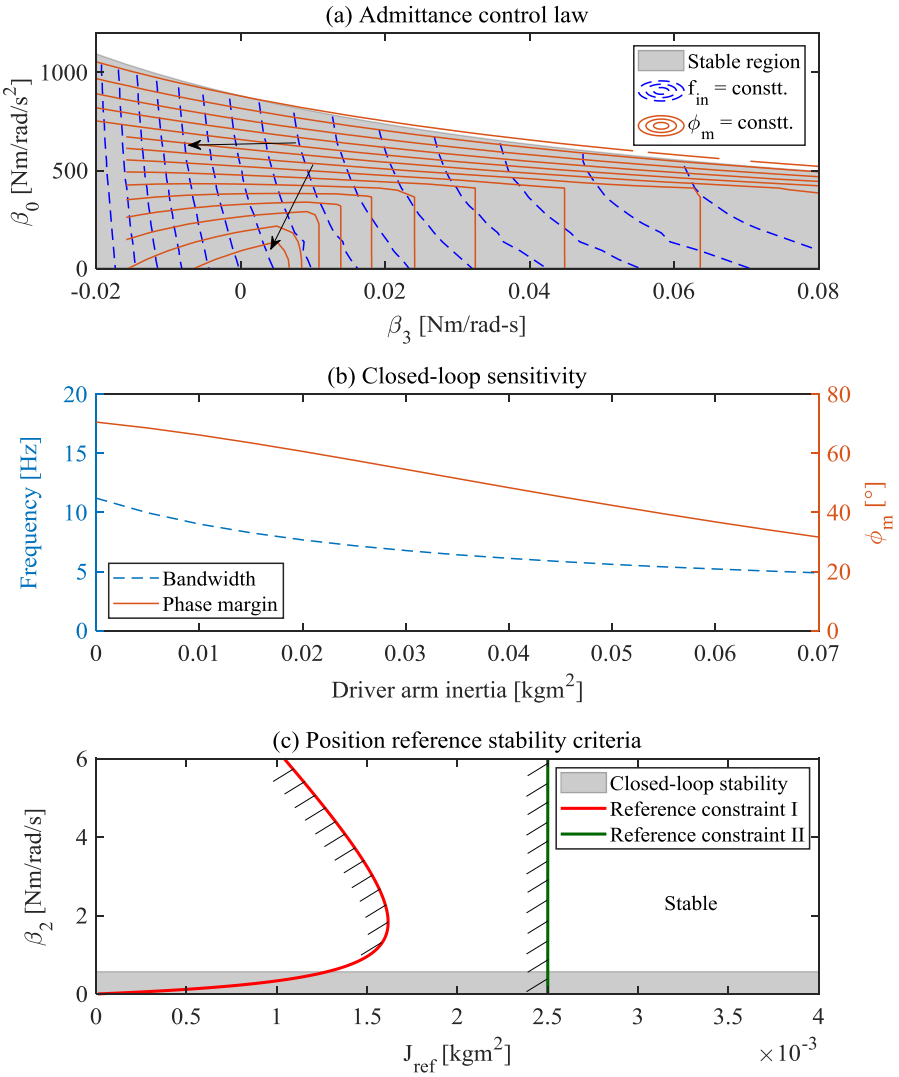

Figure 3.13: *SbW-FFb admittance control design results. (a) Stability constraint between the feedback control gains β_0-β_3 from Eq.* (3.11)*. The 'blue' colored --- lines represent constant bandwidth (f_{in}) and the 'orange' colored — lines represent constant phase margin (ϕ_m). The arrows indicate the direction of increasing f_{in} and ϕ_m. (b) Closed-loop sensitivity of driver arm inertia on f_{in} and ϕ_m. (c) The 'Reference constraint I' is stability criteria in Eq.* (3.14) *between admittance reference inertia and feedback gain β_2. The 'Reference constraint II' represents $J_{ref} \geq J_{mot}$ $\forall$ $\beta_2 \geq 0$. The unstable regions are hatched for convenience. The 'Closed-loop stability' criteria is derived using Eq.* (3.11)

.

and $\beta_3 < 0$, the bandwidth can be improved at the expense of β_0 (which substantially affects the reference tracking in steady state)' and (b) '*for a selected phase margin and $\beta_3 > 0$, the bandwidth is compromised significantly and the β_0 upper bound also reduces as shown in Eq.* (3.11)'. Hence, β_3 is selected carefully to have a sufficient inner-loop phase margin and that results in a constrained bandwidth.

$$\beta_0 < \frac{1}{i_{mp}} \left(\frac{b_s + b_k + \beta_2 i_{mp}}{J_s + J_{arm} + J_k + \beta_3 i_{mp}} \right) \left(c_k + \beta_1 i_{mp} \right) \tag{3.11}$$

The closed-loop sensitivity is discussed next. The effect of J_{arm} and v_x variation are given in Fig. 3.12(b) and (c) respectively for EPAS; and see Fig. 3.13(b) for the effect of J_{arm} variation in SbW-FFb. The results conclude that the admittance control inherently suffers with the variation in arm inertia (as the performance is reduced with increasing J_{arm} keeping the same feedback control). Although the phase margin in EPAS is not affected much, but it is not the case for SbW-FFb. Because the largest inertia is contributed by the driver arms and not by the servo motor (unlike in EPAS). Furthermore, the closed-loop EPAS plant is robust against vehicle speed variation, similar to the impedance control.

Since the outer-loop is an admittance, then the closed-loop plant is constrained to have an impedance causality. The next uncoupled stability criteria is derived using $H_{ref,\theta} = 1/(J_{ref}s^2 + b_{ref}s + c_{ref})$. Again, the stability criteria could have two possibilities. In the first case, we assume a predefined servo control bandwidth, ω_{in}, and find the J_{ref} bound (with the assumptions $b_{ref} = 0$ Nms/rad, $c_{ref} = 0$ Nm/rad and $k_{tb} \to 0$ Nms/rad). The resulting loop gain is given in Eq. (3.12) and presented in Fig. 3.9(b). For a necessary and sufficient stability condition (derived using L_θ), the inequality constraint in Eq. (3.13) provides a lower bound on J_{ref}. It signifies that how much lower inertia one could realize in the outer-loop admittance, given a certain inner-loop performance. The smaller the reference inertia, the faster the reference dynamics which the driver could sense. It can be seen graphically in Fig. 3.14(a) for EPAS system. If the driver arm inertia is higher, then the unstable region will increase and so as the J_{ref} lower bound for a given ω_{in}.

$$L_\theta = -H_{ref,\theta} H_{servo} \frac{G_{32}}{G_{22}} = \frac{1}{J_{ref}s^2} \left(\frac{1}{1 + (1/\omega_{in})s} \right) \left(\frac{((J_s + J_{arm})s^2 + b_s s)c_{tb}}{(J_s + J_{arm})s^2 + b_s s + c_{tb}} \right) \tag{3.12}$$

$$J_{ref} > \frac{J_s + J_{arm}}{b_s + k_{tb}} \left(\frac{-(J_s + J_{arm})k_{tb}\omega_{in}^2 + \left((J_s + J_{arm})c_{tb} - k_{tb}^2\right)\omega_{in}}{(J_s + J_{arm})\omega_{in}^2 + (b_s + k_{tb})\omega_{in} + c_{tb}} \right) \tag{3.13}$$

For the second possibility with a defined J_{ref}, the inner-loop is designed using β_2 such that Eq. (3.14) is fulfilled. The assumptions are $\{c_{ref}, b_{ref}, b_s, b_k, \beta_0, \beta_1, \beta_3\} = 0$. It is a necessary and sufficient stability condition for LHP closed-loop poles. Also, if we consider β_0, β_1 and β_3 using the actual control law then there is another lower bound condition on β_2 from Eq. (3.11) for the inner-loop stability. Both these conditions should be satisfied for uncoupled stability. Fig. 3.14(b) summarizes the above discussion

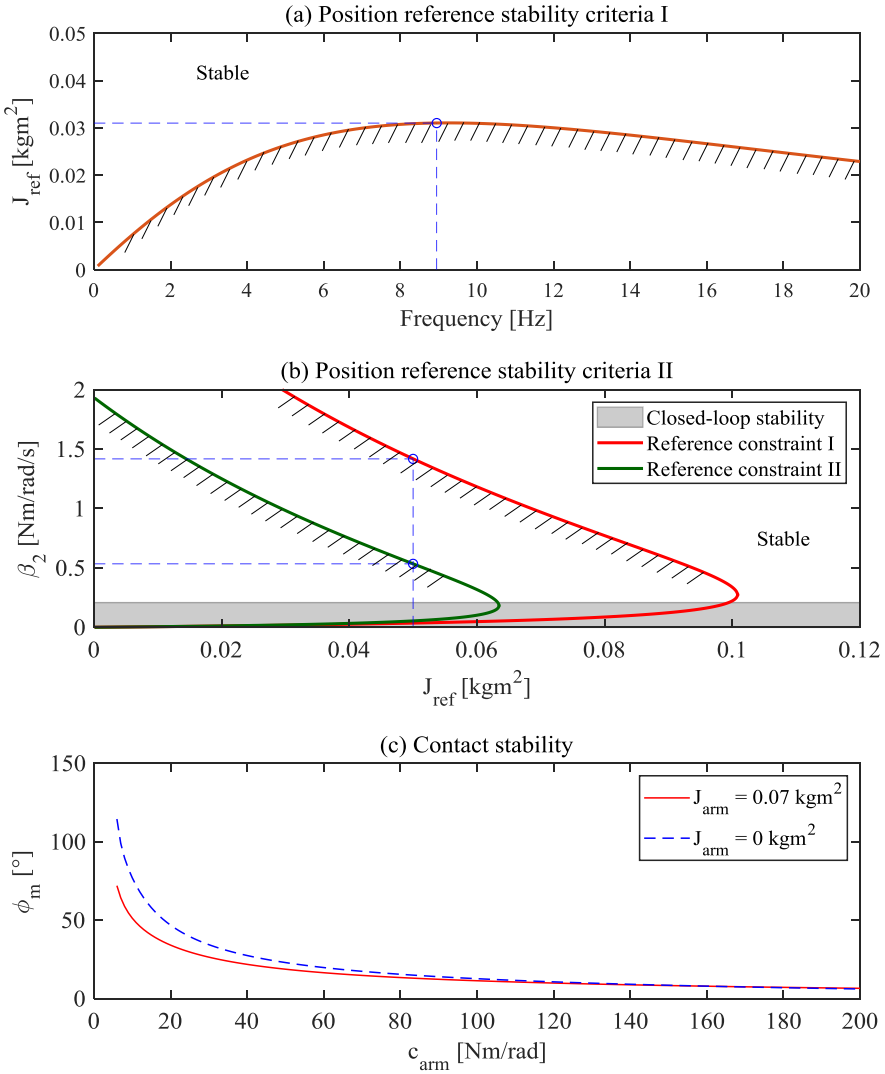

Figure 3.14: *EPAS admittance control design results. (a) The stability criteria in Eq.* (3.13) *between inner-loop bandwidth and admittance reference inertia. (b) The 'Reference constraint I' is the stability criteria in Eq.* (3.14) *between admittance reference inertia and feedback gain* β_2*. The 'Reference constraint II' represents the same equation with reduced system inertia or* $\beta_3 \neq 0$*. The 'Closed-loop stability' criteria is derived using Eq.* (3.11)*. The unstable regions are hatched for convenience. (c) The driving port admittance loop gain phase margin (robustness measure of contact stability) as a function of drivers' arm stiffness for different arm inertia.*

for EPAS. With $\beta_3 \neq 0$, the system inertia is further compensated and subsequently it relaxes the condition on β_2 as shown in the figure for the same J_{ref} (thus increasing the stable region). A similar result can be seen for SbW-FFb in Fig. 3.13(c). If the torsional compliance is assumed infinitely stiff, then the sufficient stability condition is $J_{ref} \geq J_{mot}$ [1]. Otherwise with a limited compliance, the below derived equation can be used to realize $J_{ref} < J_{mot}$ within some range of β_2.

$$\beta_2^2 + \left[\left(\frac{1-\frac{J_k}{J_{ref}}}{\frac{1}{J_s+J_{arm}}+\frac{1}{J_{ref}}}\right)\frac{c_{tb}}{k_{tb}} + k_{tb}\left(1+\frac{J_k}{J_s+J_{arm}}\right)\right]\beta_2 + \frac{c_{tb}\left(\frac{J_k}{J_s+J_{arm}}+1\right)^2}{\frac{1}{J_s+J_{arm}}+\frac{1}{J_{ref}}} > 0 \quad (3.14)$$

The coupled stability is maintained at the interaction point by ensuring the driving port admittance, $Z(s)$, to be passive. As a result, the controller parameters are selected for a positive real $Z(s)$. The contact instability is a more common phenomenon in admittance control, but we have tried to mitigate it. The loop gain $L_d = G_{arm}^{-1}Z$ (see Fig. 3.9(c)) and its respective phase margin for EPAS and SbW-FFb with varying c_{arm} is shown in Fig. 3.14(c) and Fig. 3.11. Similar to the impedance control, the designed admittance control law (with all the constraints being satisfied) guaranteed the passivity of closed-loop $Z(s)$ in EPAS (even though the plant model is not passive at higher vehicle speeds).

3.2.3 Feedback control validation

This section presents the result of the closed-loop haptic feedback control methods with driver excitation (Case I). The impedance and admittance feedback control laws were designed using the previous section. The linearized reference generator parameters are assumed to be given, although they have been estimated from the actual vehicles' open loop control response which will be discussed in the next section.

For EPAS, the steering feedback controller is implemented in CarMaker using the existing motor current control model. The frequency response of torsion bar torque to pinion angular position and velocity are shown in Fig. 3.15(a) and (b) respectively. The reference tracking shows a reasonable behavior, refer Fig. 3.15(c), since the controllers offer a sufficient bandwidth within the drivers' steering excitation range. A similar result for SbW-FFb was obtained from the experiments. The torsion bar torque to pinion angular position, velocity and reference to actual control variable FRF are shown in Fig. 3.16 respectively. The FRF results clearly indicate an improvement with impedance and admittance control in comparison to the open loop control.

3.2.4 Reference model for driver excitation

Case I reference generator is discussed here as shown in Fig. 3.6. Although we have introduced the LTI second-order reference in Section 3.2.2 for simplicity, but the driver experiences a somewhat more detailed dynamics such as tire and vehicle response,

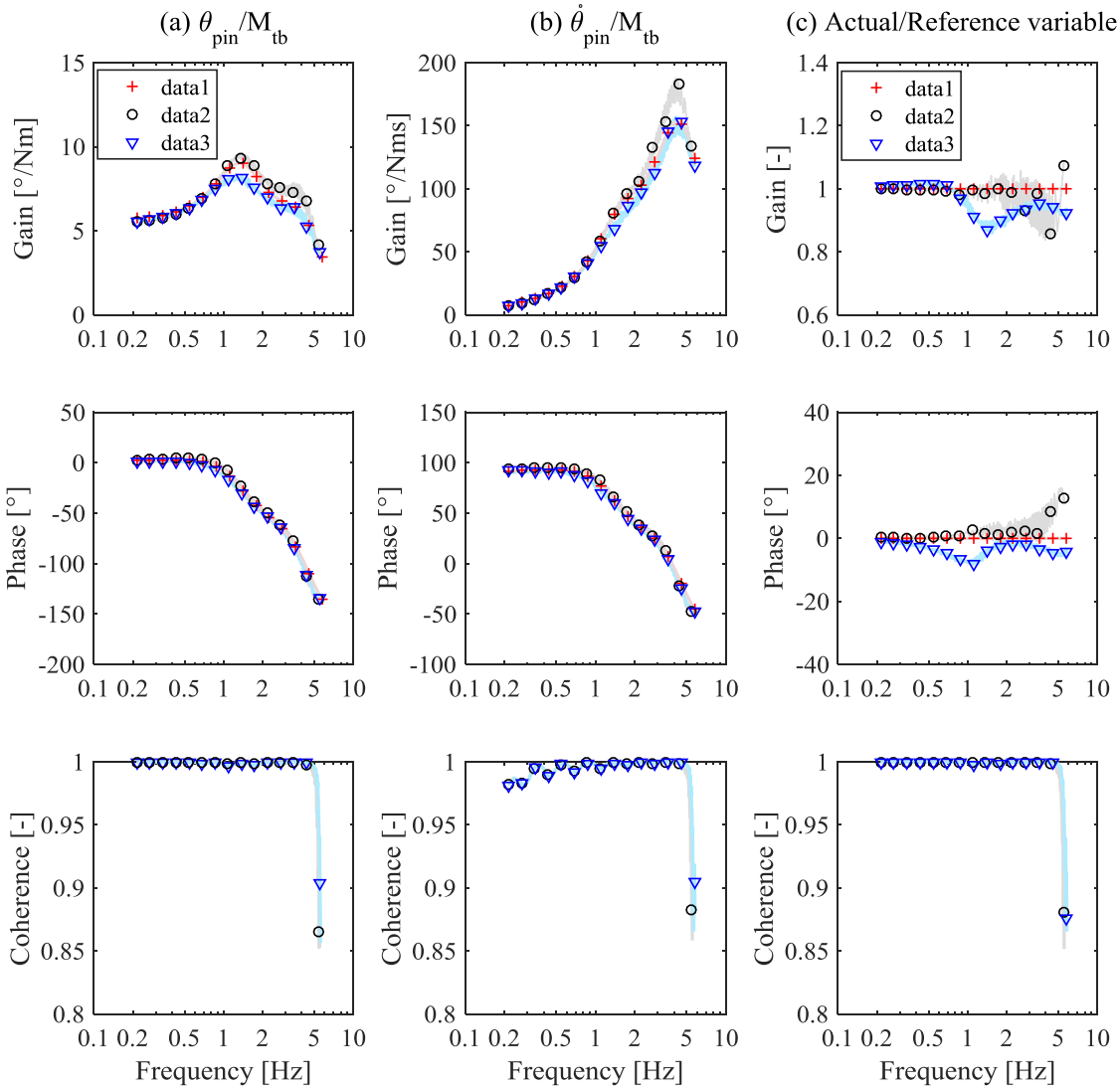

Figure 3.15: *Post-processed EPAS simulation result of torsion bar torque to (a) pinion angular position and (b) angular velocity frequency response at 75 km/h vehicle speed. The plot details are: data1 – reference, data2 – impedance control and data3 – admittance control. (c) Frequency response of reference to actual control variable. The plot details are: data1 – reference (gain = 1 and phase = 0°), data2 – $M_{tb}/M_{tb,ref}$ for impedance control and data3 – $\theta_{pin}/\theta_{pin,ref}$ for admittance control.*

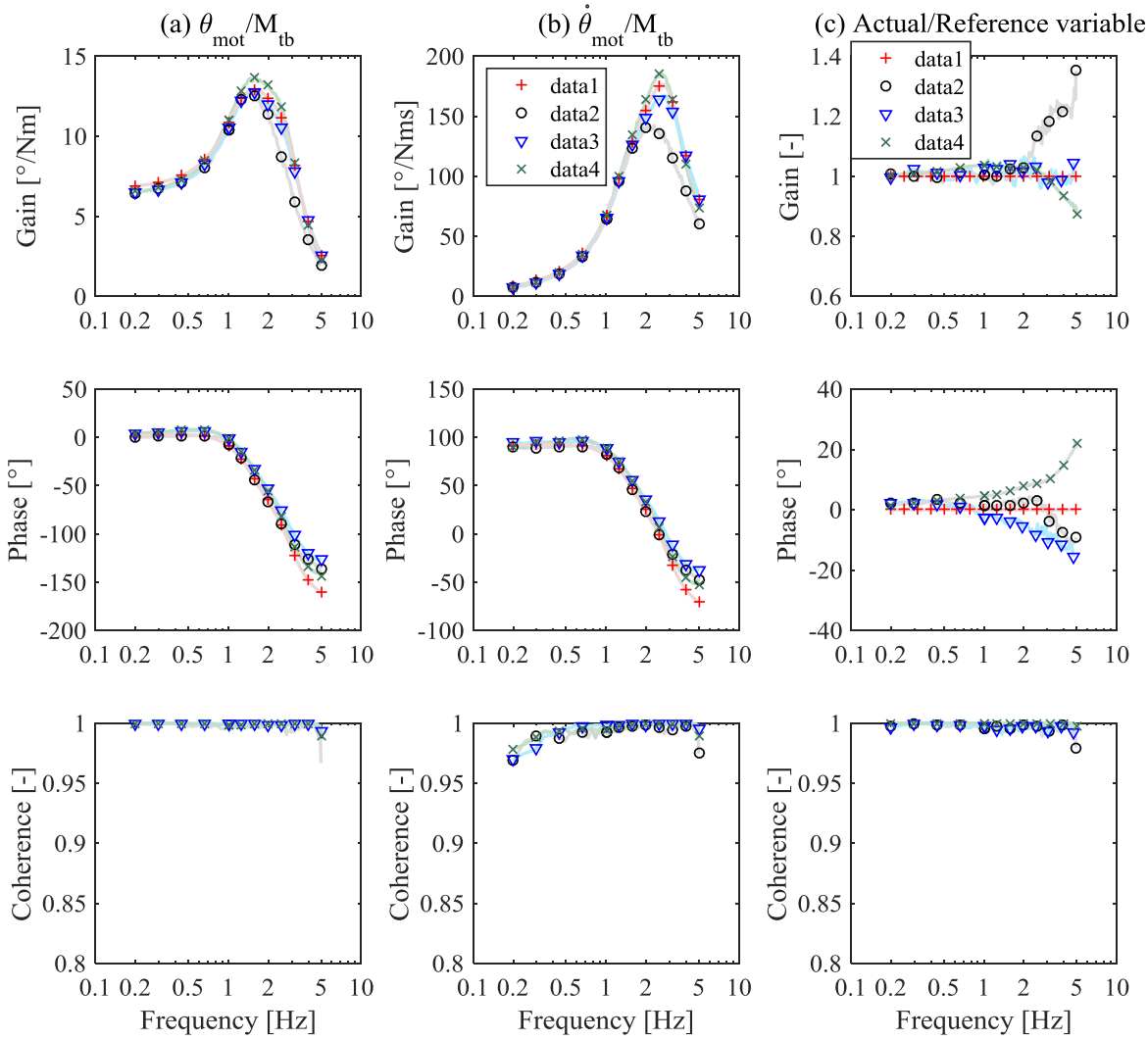

Figure 3.16: *Post-processed SbW-FFb test rig result of torsion bar torque to (a) motor angular position and (b) angular velocity frequency response. The plot details are: data1 – reference (at 75 km/h vehicle speed), data2 – open loop control, data3 – impedance control and data4 – admittance control. (c) Frequency response of reference to actual control variable. The plot details are: data1 – reference (gain = 1 and phase = 0°), data2 – $M_{tb}/M_{tb,ref}$ for open loop control, data3 – $M_{tb}/M_{tb,ref}$ for impedance control and data4 – $\theta_{mot}/\theta_{mot,ref}$ for admittance control.*

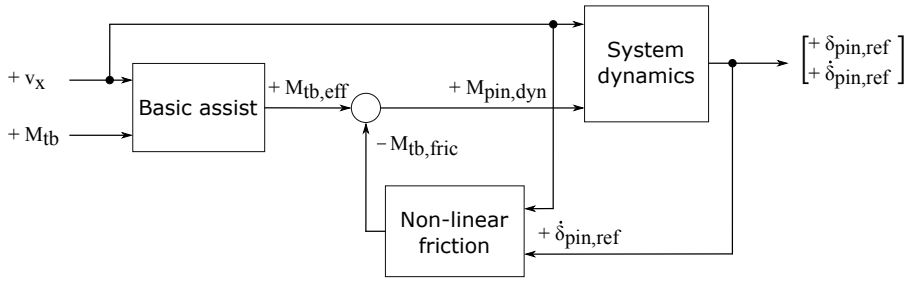

(a) Reference generator for admittance control

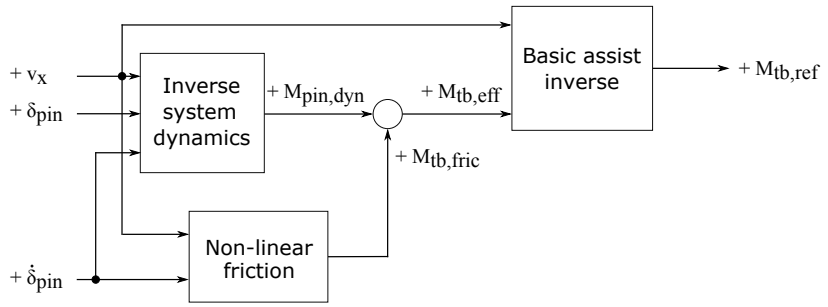

(b) Reference generator for impedance control

Figure 3.17: *The reference generator block diagrams for (a) admittance and (b) impedance control respectively (figure reproduced from Paper D). Here, δ_{pin} symbolically represents θ_k.*

open loop functions as shown in Fig. 3.2. A brief explanation is given below, but the details are provided in Paper D where we have presented a method to extract the reference model parameters from a state-of-the-art steering system (limited to 4 m/s^2 lateral acceleration). The paper also shows validation result of the complete reference generator with their respective feedback control laws. The three important elements in the reference model are as follows.

(a) System dynamics: It consists of the linear estimated steering response (based on a particular road feedback and vehicle characteristic). The reference inertia, damping and stiffness functions can be manipulated here.

(b) Basic assist: This defines the typical non-linear quasi-static relation between the steering rack force (or equivalent to assist motor torque) and torsion bar torque.

(c) Non-linear friction: It is responsible for creating the effect of Coulomb friction torque as a function of angular velocity.

The torsion bar torque is a primary input to the admittance reference for generating the reference angular position and velocity, refer Fig. 3.17(a). Whereas the impedance reference is complementary to the admittance reference as seen in Fig. 3.17(b), based on causal analysis. The angular position and velocity signals are used in inverse system

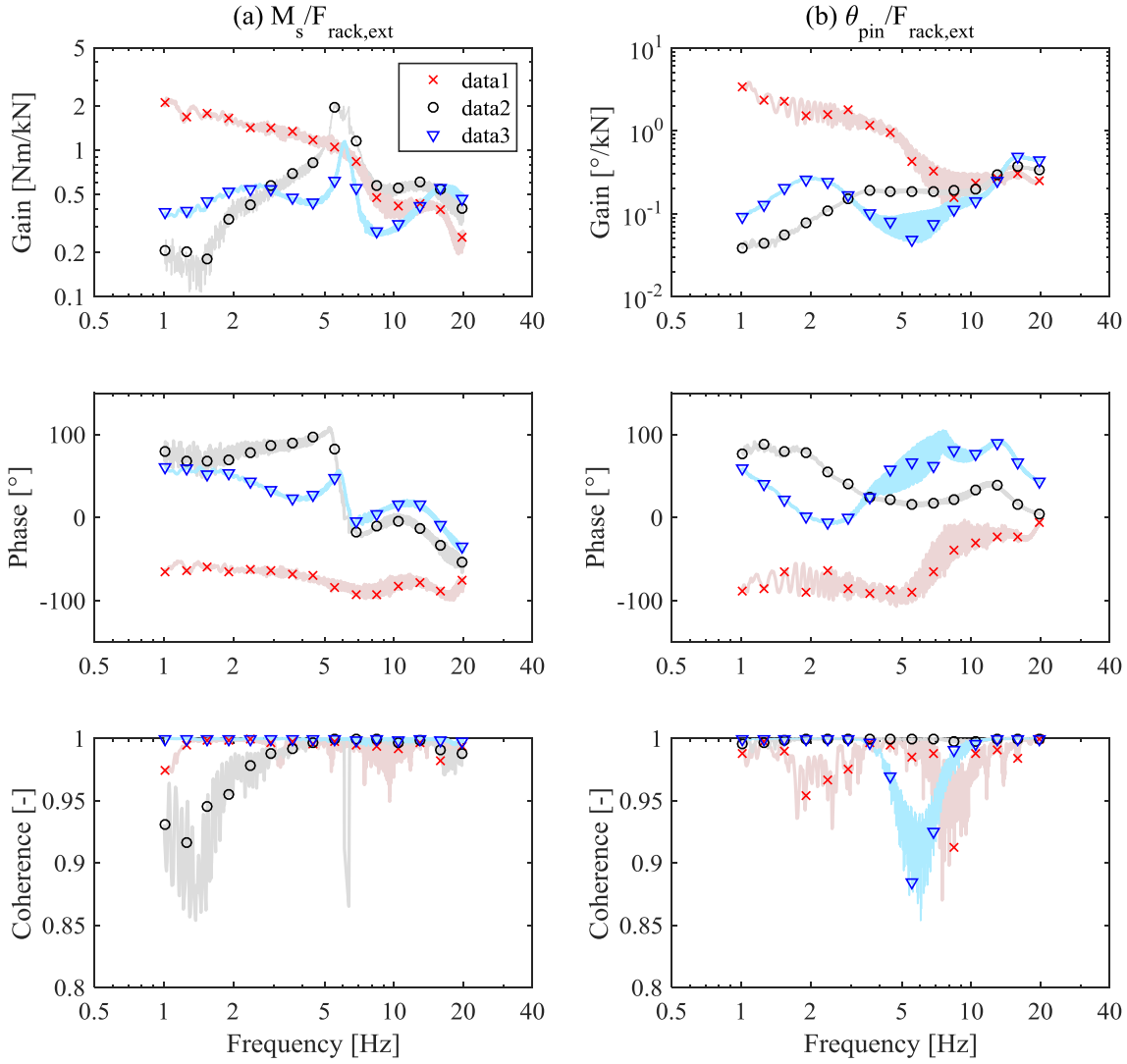

Figure 3.18: *Post-processed EPAS simulation result of external steering rack force to (a) steering torque and (b) pinion angle frequency response at 75 km/h vehicle speed. The plot details are: data1 – open loop control, data2 – impedance control and data3 – admittance control. The closed-loop feedback control methods provide road feedback attenuation.*

dynamics for angular acceleration estimation. Although the impedance and admittance reference models, as developed in Paper D, are limited to low lateral acceleration levels, the presented layouts are still valid in the entire operating range. For higher vehicle lateral acceleration, vehicle and tires' non-linearity need to be considered in the system dynamics.

3.2.5 Reference model for road excitation: The step forward

Up till now we have generated a virtual steering feedback based on the driver excitation reference model. The next step is to introduce useful road excitation. However this is not considered in the present thesis, and will be considered in the future investigations.

A short overview of the road excitation is covered in this section. At first we consider the EPAS system, where the external road excitation is one of the disturbance inputs to the plant model. The open loop control has its shortcoming regarding this, as discussed in Section 3.1. The effect is amplified in closed-loop control, since these excitation are further attenuated as controllers' disturbance rejection. The external steering rack force decoupling results in Fig. 3.18(a) and (b) for Case II(a) and II(b) respectively explain this phenomenon more clearly. As it can be seen in the figure, the steering torque and pinion angle response are rather attenuated as compared to the open loop control. This is not a desirable characteristic for an actual road feedback feel. It is however a step towards realizing the closed-loop control. Our aim is to maximize the inner-loop bandwidth (be it impedance or admittance control), and then feed the external road excitation via the reference generator. This will require either a real-time precisely estimated or measured steering rack force signal for the reference generator. For SbW-FFb system, the requirements are exactly the same and so as the possible approach.

Chapter 4

Overlaying vehicle motion control request

This chapter is dedicated for merging haptic feedback control and vehicle motion control functions. Haptic feedback control is covered in the previous chapter. Vehicle motion control functions (such as lane keeping aid, pilot assist, etc.) request a reference pinion angle in a typical EPAS system. The pinion angle controller (or admittance control) applies the required motor torque to achieve the desired vehicle positioning on the road. These kind of interventions are defined under vehicle excitation source category (refer Case III definition in Chapter 3). The details on vehicle motion control request and its position controller are out of context for this thesis. The question under investigation is how to overlay these interventions with haptic feedback control. For our research, we consider two overlay possibilities via either motor torque in open loop or angular position in closed-loop. For SbW, the focus is on the FFb system. The vehicle motion control request on the steering rack actuator can be similarly realized on the FFb system either fully or partially or completely decoupled. However it should ultimately feel natural and a part of the FFb during an intervention. We will not quantify what exactly needs to be realized, but the question on how to realize the request on the FFb actuator is dealt with.

4.1 Open loop motor torque overlay

The state-of-the-art motor torque overlay with open loop haptic feedback control is shown in Fig. 4.1(a). In this architecture, a separate angular position controller is required for tracking the reference.

We will look into Case III(a), where the external motor torque request excites the steering system with driver following the straight line path, basically to objectify the influence on steering torque. The result is shown in Fig. 4.2(a). The EPAS plots have been normalized with respect to the transmission ratio i_{mp} for a fair comparison to SbW-FFb. The following observations can be concluded.

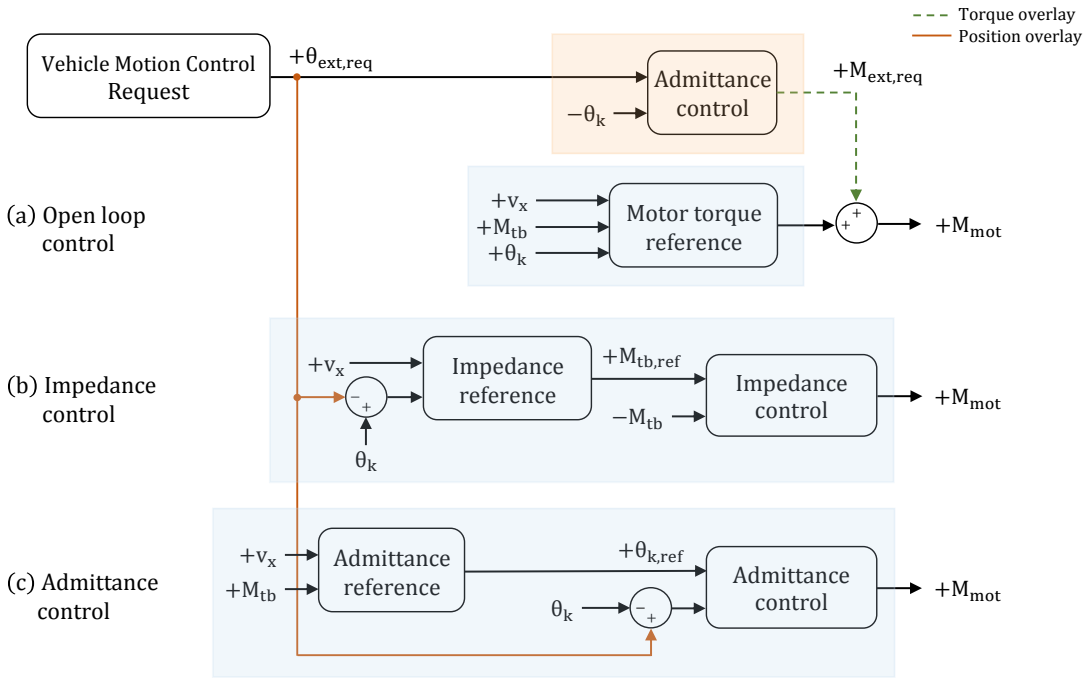

Figure 4.1: *Architecture for (a) open loop motor torque overlay and angular position overlay in (b) impedance and (c) admittance control, representing the merging of haptic feedback control and vehicle motion control functions. Open loop motor torque overlay requires a separate admittance (or position) control for realizing the vehicle motion control request.*

(a) The open loop EPAS control software (plot '*data*1' with + markers) partially attenuates the low frequency intervention. For a given vehicle motion control request via motor torque overlay, the haptic feedback response is constrained because of the single actuator and an indirect interaction between the two functions.

(b) The open loop SbW-FFb control (plot '*data*2' with ○ markers) directly translates $M_{ext,req}$ on the steering wheel with a bandwidth around 5 Hz. One could easily alter the response depending on the haptic feedback preferences, because of a separate vehicle motion control actuation.

(c) A typical motor torque overlay, regardless of EPAS or SbW-FFb, in closed-loop control (plot '*data*3' with △ markers) would attenuate the low frequency excitation. This result is similar to the road excitation attenuation response in closed-loop EPAS as shown in Fig. 3.18. Closed-loop motor torque overlay would result in a conflict between the two functions and as a result in EPAS, the vehicle motion control request could not be achieved in a straightforward way.

A typical disturbance attenuation (or rejection) response at lower frequencies is equivalent to '$-1/s$' transfer function. Therefore the phase delay starts around 90° for closed-loop cases, as compared to approximately 0° for open loop.

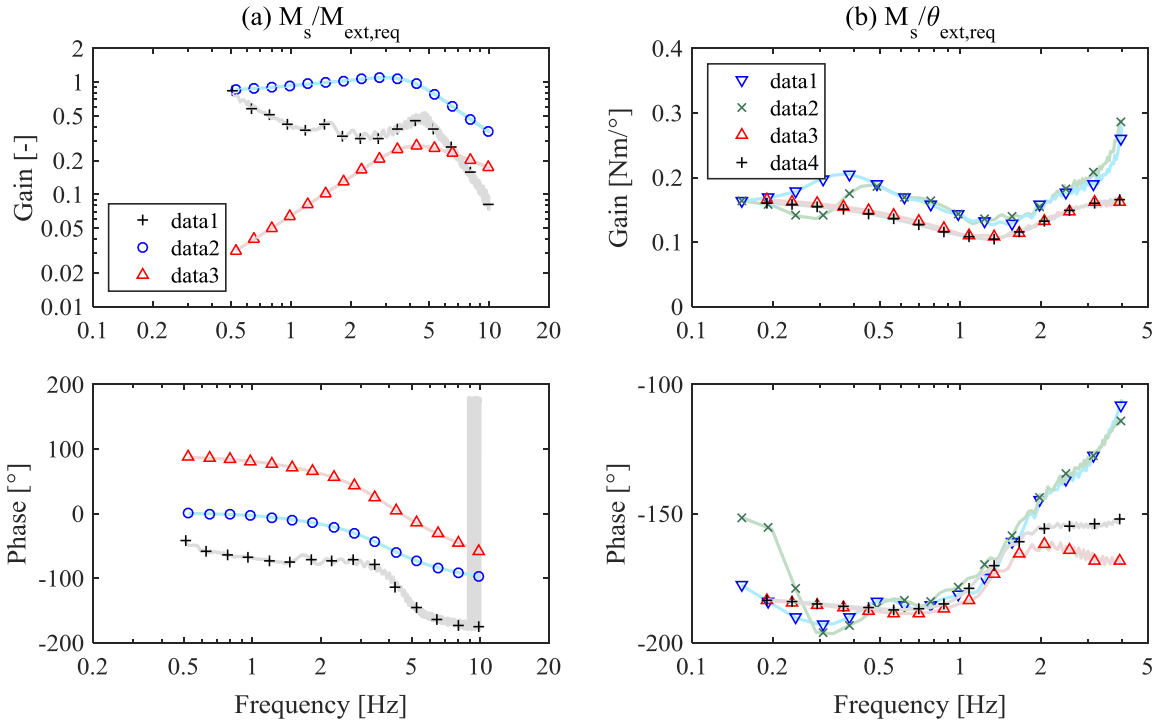

Figure 4.2: *(a) Motor torque overlay: Frequency response of $M_s/M_{ext,req}$ for test Case III(a) at 75 km/h vehicle speed. The plot details are: data1 – EPAS open loop, data2 – SbW-FFb open loop and data3 – a typical closed-loop control. (b) Angular position overlay: Frequency response of $M_s/\theta_{ext,req}$ for test Case III(a) at 75 km/h vehicle speed. The plot details are: data1 – EPAS impedance control, data2 – EPAS admittance control, data3 – SbW-FFb impedance control and data4 – SbW-FFb admittance control.*

4.2 Closed-loop angular position overlay

A straightforward way to realize the vehicle motion control request in closed-loop control is angular position overlay, see Fig. 4.1(b) and (c) for impedance and admittance control respectively. In impedance control, the position overlay is done at the reference (on the outer-loop) and at the feedback control (on the inner-loop) for admittance control. For both, it would result in a similar response mathematically which can be proven using Eq. 3.9. The frequency response results for Case III(a) are presented in Fig. 4.2(b).

The angular position overlay understandably causes a direct influence of the steering torque. A very similar and consistent frequency response ($M_s/\theta_{ext,req}$) is obtained in both the closed-loop steering systems. Same as before, the haptic feedback response is constrained for EPAS and cannot be altered without affecting the vehicle motion control request. Whereas in SbW-FFb, the response could easily be manipulated independent of the steering rack actuation. The important point is that the two functions are realized in a sequential manner, thus directly interdependent.

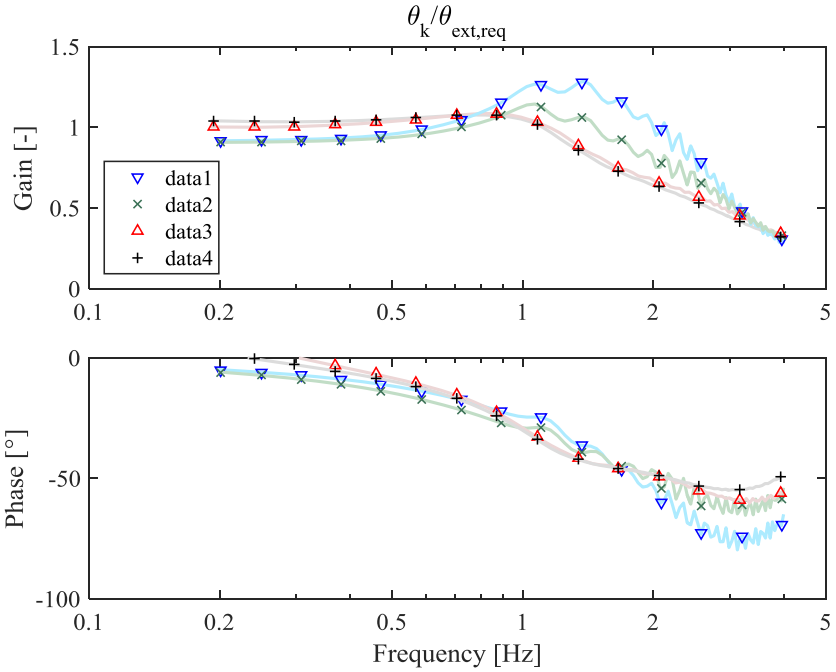

Figure 4.3: *Angular position overlay: Frequency response of $\theta_k/\theta_{ext,req}$ for test scenario Case III(b) at 75 km/h vehicle speed, where $k = \{pin,mot\}$ for EPAS and SbW-FFb respectively. The plot details are: data1 – EPAS impedance control, data2 – EPAS admittance control, data3 – SbW-FFb impedance control and data4 – SbW-FFb admittance control.*

Another interesting feature about the angular position overlay is, the closed-loop haptic feedback layout (both impedance and admittance) behaves as a position or admittance control without the driver-in-the-loop for vehicle motion control request. Thus, it fulfills the requested angular position task with a certain performance. This is evaluated under test scenario Case III(b), refer Fig. 4.3 for frequency response results. The equivalent admittance control bandwidth is approximately $1.5 - 2$ Hz for both the systems. Hence, the low frequency vehicle motion control request could be realized via the haptic feedback control. It should also be noted that the admittance haptic feedback control from Fig. 4.2(c) inherently has higher inner-loop bandwidth (as described in Chapter 3). However, the resulting bandwidth for the vehicle motion control request is reduced due to slower (admittance) reference dynamics on the outer-loop.

Chapter 5

Summary

In this chapter, we summarize the thesis with a discussion, the conclusions highlighted in previous chapters and the required future work to complete the development of the closed-loop steering feedback control function.

5.1 Discussion and conclusion

After a thorough analysis on the topic of haptic feedback control for different steering systems, we revisit the research questions from the introduction chapter in Section 1.2 and condense them as follows.

(a) How to represent the reference steering feedback response with different excitation sources?

(b) What can be concluded after investigating and comparing the closed-loop possibilities in terms of their performance, stability and robustness?

(c) How to overlay the haptic feedback control and vehicle motion control functions in a closed-loop setting?

Questions (a) and (b) are discussed in Chapter 3, whereas Chapter 4 is dedicated to question (c). In the final envisioned steering feedback control function, these questions are interdependent on each other. This is due to, since they are realized via the same haptic controller as oppose to a parallel structure in open loop control.

For question (a), the higher level control is under consideration. We have different sources of excitation for the reference feedback as shown in a state-of-the-art steering system. To understand the effect of each, we have also introduced a set of useful test cases in Chapter 3. At first, the influence of *driver excitation* in the higher level control is explained in Section 3.2.4. Regrading the same, we have presented a methodology to extract the reference model parameters from a vehicle equipped with a typical steering system using standard open-loop driving maneuvers. These parameters, once estimated,

Table 5.1: *Performance (in terms of controller bandwidth) and robustness (in terms of phase margin) comparison of closed-loop control for electric power assisted steering (EPAS) and steer-by-wire force-feedback (SbW-FFb) systems. The '→' indicates increasing driver arm inertia from* 0 kgm^2 *to* 0.07 kgm^2.

System	Closed-loop control	Bandwidth (Hz)	Phase margin (°)
EPAS	Impedance	34 → 30	40 → 30
SbW-FFb	Impedance	10	32
EPAS	Admittance	10 → 5	45
SbW-FFb	Admittance	11 → 5	70 → 30

can be used in the provided higher level control layout to meet the desired steering feedback response in a closed-loop setting. It should be noted that the driver excitation is limited to 5 Hz. The second excitation source is *road excitation*. This has not been considered in this thesis but will be covered in the future. With the existing higher level control, the effect of road excitation is attenuated by the closed-loop setting in electric power assisted steering (see Section 3.2.5). Hence, only a virtual steering feedback is obtained based on the driver excitation. From the literature, it is well known that the external road feedback to measured driver torque frequency response requirement should be up to 20 Hz. This implies that the inner-loop of the haptic feedback control (defined by the lower level control) has an ideal requirement of the controller bandwidth within this range.

The answers to question (b) are attributed to the lower level control. Their analysis is described in Section 3.2.2, along with the results in Section 3.2.3. The performance of the lower level control can be understood in combination with the hardware setup, in short 'closed-loop plant'. The different objectives of the closed-loop plant (tracking, stability and robustness) are dependent on each other. Understandably the designed closed-loop controllers ensure stability, but the tracking performance and robustness can be judged on the basis of controller bandwidth and open loop phase margin respectively. These values are given in Table 5.1, with varying driver arm inertia. Impedance (or torque) control shows better performance and more robustness as compared to admittance (or position) control for both systems. In a force-feedback system, the driver arm inertia is the main contributor towards the system impedance, as compared to the equivalent servo motor inertia in an electric power assisted steering. As a result, the closed-loop system not only significantly looses performance, but also robustness measure with increasing arm inertia. The admittance control certainly needs improvement to meet the desired steering feedback requirement.

Chapter 4 discusses about question (c) and deals with the third source of excitation, vehicle motion control function. In open loop architecture, we have a separate admittance or position controller for this and finally an overlay on the motor torque signal (refer Fig. 4.1). Here, the haptic feedback response is not explicitly considered during

these interventions and typically a byproduct. Whereas in closed-loop, it is possible to realize vehicle motion control request *via* the haptic feedback control using the angular position signal overlay. There are two advantages: (i) the two functions directly interact with each other and thus provides a better steering torque response, when driver is in the loop and (ii) the haptic feedback impedance and admittance control both behave as a position controller for vehicle motion control function with driver out of the loop.

It should also be noted that the results from coupled stability analysis (in Section 3.2.2) are valid for similar closed-loop interconnected systems such as hardware-in-the-loop test rigs, force-feedback in driving simulator, etc. Based on the discussion above and Chapter 3 and 4, some general conclusions can be derived as shown below, connected to the research questions.

(a) Lower level control:

- Better inner-loop (or closed-loop) performance in impedance control than admittance control. The admittance control, in general, is affected by higher and/or variable mechanical (or hardware) impedance.
- The linear time invariant admittance control is relatively less robust than impedance control for variable mechanical impedance. Hence, the performance and robustness are consequently affected.
- The interdependent objectives: (i) reference tracking, (ii) hardware impedance compensation and (iii) robustness could inherently conflict with each other in admittance control. However in impedance control, these objectives can be simultaneously satisfied.

(b) Higher level control:

- It is possible to realize faster reference dynamics (on the outer-loop) in admittance control than impedance control; assuming the admittance closed-loop control bandwidth (on the inner-loop) is sufficiently high.
- For non-linear Coulomb friction dynamics, the impedance reference requires a feedforward implementation as compared to the feedback connection in the admittance reference.

(c) Comparatively easier to realize the angular position overlay in a closed-loop setting, for merging haptic feedback control and vehicle motion control functionalities, than open loop control.

5.2 Future work

The reference steering feedback response in the higher level control (regardless of the steering system) needs significant development. Some of the important elements, which should be taken care of as next steps, are as follows:

- To append the driver excitation reference generator for higher vehicle lateral acceleration range (by including tire and vehicle non-linearity).
- Development of a robust steering rack force observer for realization of external road excitation in the reference generator.
- To improve the steering feedback response for lower vehicle speed range (or parking maneuvers).

Similarly, the lower level control will be investigated further on the following aspects.

- Improving the performance and robustness of admittance control in electric power assisted steering system. This is to compensate the equivalent steering rack mechanical impedance with multivariable feedback control approach (by including torsion bar torque signal).
- Improving the performance and robustness of admittance control in force-feedback system. This is to overcome the drivers' arm inertia uncertainty with multivariable feedback control approach (by including torsion bar torque signal).

The vision is to develop the closed-loop haptic controller, for a personalized steering feedback response. Basically, it means that the driver could choose a weighting on different excitation sources. For instance, a virtual steering feedback is provided in case the driver wants to completely isolate the external road feedback. On the contrary, a more realistic road feedback is provided to the driver for limit handling maneuvers.

This thesis has presented the shortcoming of the existing open loop control (for electric power assisted steering and steer-by-wire force-feedback systems) and enabled a step towards understanding of closed-loop steering feedback control function. The improvement points, as mentioned in this chapter, will be considered in the next steps. The experiments will also be performed to evaluate the closed-loop steering feedback control function on a prototype vehicle, with real-time test equipment, for both the steering systems.

Bibliography

[1] G. Aguirre-Ollinger, J. E. Colgate, M. A. Peshkin, and A. Goswami, *Design of an active one-degree-of-freedom lower-limb exoskeleton with inertia compensation*, International Journal of Robotics Research, 30 (2011), pp. 486–499.

[2] G. Aguirre-Ollinger, J. E. Colgate, M. A. Peshkin, and A. Goswami, *Inertia compensation control of a one-degree-of-freedom exoskeleton for lower-limb assistance: Initial experiments*, IEEE Transactions on Neural Systems and Rehabilitation Engineering, 20 (2012), pp. 68–77.

[3] A. Badawy, J. Zuraski, F. Bolourchi, and A. Chandy, *Modeling and Analysis of an Electric Power Steering System*, International Congress and Exposition Detroit, Michigan March 1-4, 1999 400, 1999 (1999).

[4] N. Bajcinca, *Haptic Control for Steer-by-Wire Systems*, Proceedings of the 2003 IEEE/RSJ Intl. Conference on Intelligent Robots and Systems, (October 2003).

[5] A. Balachandran and J. C. Gerdes, *Designing steering feel for steer-by-wire vehicles using objective measures*, IEEE/ASME Transactions on Mechatronics, 20 (2015), pp. 373–383.

[6] A. Bolopion and S. Régnier, *A review of haptic feedback teleoperation systems for micromanipulation and microassembly*, IEEE Transactions on Automation Science and Engineering, 10 (2013), pp. 496–502.

[7] Bosch Group, *Zf lenksysteme servolectric*. `http://www.bosch-presse.de/pressportal/zip?country=de&language=en&docId=41849`. Accessed: 2019-04-03.

[8] Bosch Mobility Solutions, *Servolectric electric power steering system*. `https://www.bosch-mobility-solutions.com/media/global/products-and-services/passenger-cars-and-light-commercial-vehicles/steering-systems/servolectric-steering-systems/folder_for_steering_systems_pkw.pdf`. Accessed: 2019-04-03.

[9] M. Bröcker, *New control algorithms for steering feel improvements of an electric powered steering system with belt drive*, Vehicle System Dynamics, 44 (2006), pp. 759–769.

[10] C. Carignan and K. Cleary, *Closed-loop force control for haptic simulation of virtual environments*, Haptics-e, 1 (2000), pp. 1–14.

[11] D. J. Cole, *A path-following driver-vehicle model with neuromuscular dynamics, including measured and simulated responses to a step in steering angle overlay*, Vehicle System Dynamics, 50 (2012), pp. 573–596.

[12] E. Colgate and N. Hogan, *An analysis of contact instability in terms of passive physical equivalents*, Proceedings, 1989 International Conference on Robotics and Automation, (1989), pp. 404–409.

[13] J. E. Colgate, *Robust control of dynamically interacting systems*, International Journal of Control, 48 (1988), pp. 65–88.

[14] J. E. Colgate, *Strictly positive real admittances for coupled stability*, Journal of the Franklin Institute, 329 (1992), pp. 429 – 444.

[15] N. Dahlström, *Pilot training in our time use of flight training devices and simulators*, Aviation, 12 (2008), pp. 22–27.

[16] N. Dahlström, S. Dekker, R. van Winsen, and J. Nyce, *Fidelity and validity of simulator training*, Theoretical Issues in Ergonomics Science, 10 (2009), pp. 305–314.

[17] C. Dannöhl, S. Müller, and H. Ulbrich, *H_∞-control of a rack-assisted electric power steering system*, Vehicle System Dynamics, 50 (2012), pp. 527–544.

[18] E. De Vlugt, A. C. Schouten, F. C. Van Der Helm, P. C. Teerhuis, and G. G. Brouwn, *A force-controlled planar haptic device for movement control analysis of the human arm*, Journal of Neuroscience Methods, 129 (2003), pp. 151–168.

[19] S. Fankem and S. Müller, *A new model to compute the desired steering torque for steer-by-wire vehicles and driving simulators*, Vehicle System Dynamics, 52 (2014), pp. 251–271.

[20] G. Fontaras, N.-G. Zacharof, and B. Ciuffo, *Fuel consumption and co2 emissions from passenger cars in europe laboratory versus real-world emissions*, Progress in Energy and Combustion Science, 60 (2017), pp. 97–131.

[21] V. Govender and S. Müller, *Modelling and Position Control of an Electric Power Steering System*, IFAC-PapersOnLine, 49 (2016), pp. 312–318.

[22] D. Gualino and I.-J. Adounkpe, *Force-Feedback System Design for the Steer-By-Wire: Optimisation and Performance Evaluation*, 2006 IEEE Intelligent Transportation Systems Conference, (2006), pp. 181–187.

[23] M. Harrer and P. Pfeffer, *Steering Handbook*, Springer International Publishing AG, 2017.

[24] R. Hayama, S. Kawahara, and S. Nakano, *Resistance torque control for steer-by-wire system to improve human machine interface*, Vehicle System Dynamics, 48 (2010), pp. 1065–1075.

[25] R. T. Hays, J. W. Jacobs, C. Prince, and E. Salas, *Flight simulator training effectiveness: A meta-analysis*, Military Psychology, 4 (1992), pp. 63–74.

[26] Hitachi Automotive Systems Americas, Inc., *Belt drive electric power steering system.* `http://www.hitachi-automotive.us/Products/oem/DCS/Steering/index.htm`. Accessed: 2019-04-03.

[27] N. Hogan and S. P. Buerger, *Robotics and Automation Handbook, Chapter 19 Impedance and Interaction Control*, CRC Press, LLC, 2005.

[28] H. Hsu and M. Harrer, *The New Steering System in the 911 Porsche Carrera Optimized Design of a Steering System for Sportcars*, 21st Aachen Colloquium Automobile and Engine Technology, (2012).

[29] T. H. Hu, C. J. Yeh, S. R. Ho, T. H. Hsu, and M. C. Lin, *Design of control logic and compensation strategy for electric power steering systems*, 2008 IEEE Vehicle Power and Propulsion Conference, VPPC 2008, (2008), pp. 1–6.

[30] D. I. Katzourakis, D. A. Abbink, E. Velenis, E. Holweg, and R. Happee, *Driver's arms' time-variant neuromuscular admittance during real car test-track driving*, IEEE Transactions on Instrumentation and Measurement, 63 (2014), pp. 221–230.

[31] H. K. Khalil, *Nonlinear systems; 3rd ed.*, Prentice-Hall, Upper Saddle River, NJ, 2002. The book can be consulted by contacting: PH-AID: Wallet, Lionel.

[32] K. Kosuge, Y. Fujisawa, and T. Fukuda, *Control of mechanical system with man-machine interaction*, in Proceedings of the IEEE/RSJ International Conference on Intelligent Robots and Systems, vol. 1, July 1992, pp. 87–92.

[33] D. A. Lawrence, *Stability and Transparency in Bilateral Teleoperation*, IEEE Transactions on Robotics and Automation, 9 (1993), pp. 624–637.

[34] M. Ljungberg, M. Nybacka, G. Gil Gómez, and D. Katzourakis, *Electric power assist steering system parameterization and optimisation employing computer-aided engineering*, in SAE 2015 World Congress & Exhibition, SAE International, April 2015.

[35] A. M. Okamura, *Haptic feedback in robot-assisted minimally invasive surgery*, Current Opinion in Urology, 19 (2008), pp. 102–107.

[36] C. Ott, R. Mukherjee, and Y. Nakamura, *Unified impedance and admittance control*, Proceedings - IEEE International Conference on Robotics and Automation, (2010), pp. 554–561.

[37] P. E. Pfeffer, M. Harrer, and D. N. Johnston, *Modelling of a Hydraulic Steering System*, FISITA, (2006).

[38] R. O. A. Rehnmark, H. Aldridge, R. S. Askew, R. R. Burridge, W. Bluethmann, M. Diftler, C. Lovchik, D. Magruder, and F., *Robonaut : NASA's Space Humanoid*, IEEE Intelligent Systems and their Applications, 15 (2000), pp. 57–63.

[39] M. Rothhmel, J. IJkema, and L. Drugge, *Influencing driver chosen cornering speed by means of modified steering feel*, Vehicle System Dynamics, 52 (2014), pp. 522–538.

[40] A. C. Schouten, E. de Vlugt, J. J. B. van Hilten, and F. C. T. van der Helm, *Design of a torque-controlled manipulator to analyse the admittance of the wrist joint*, Journal of Neuroscience Methods, 154 (2006), pp. 134–141.

[41] S. Skogestad and I. Postlethwaite, *Multivariable feedback control: analysis and design*, International Journal of Robust and Nonlinear Control, 8 (2001), p. 575.

[42] J. Timings and D. Cole, *Robust lap-time simulation*, Proceedings of the Institution of Mechanical Engineers, Part D: Journal of Automobile Engineering, 228 (2014), pp. 1200–1216.

[43] P. M. van Leeuwen, S. de Groot, R. Happee, and J. C. F. de Winter, *Differences between racing and non-racing drivers: A simulator study using eye-tracking*, PLOS ONE, 12 (2017), pp. 1–19.

[44] M. Von Groll, S. Mueller, T. Meister, and R. Tracht, *Disturbance compensation with a torque controllable steering system*, Vehicle System Dynamics, 44 (2006), pp. 327–338.

[45] C. R. Wagner and R. D. Howe, *Force feedback benefit depends on experience in multiple degree of freedom robotic surgery task*, IEEE Transactions on Robotics, 23 (2007), pp. 1235–1240.

[46] J. G. Wildenbeest, D. A. Abbink, C. J. Heemskerk, F. C. Van Der Helm, and H. Boessenkool, *The impact of haptic feedback quality on the performance of teleoperated assembly tasks*, IEEE Transactions on Haptics, 6 (2013), pp. 242–252.

[47] J. G. Wildenbeest, R. J. Kuiper, F. C. Van Der Helm, and D. A. Abbink, *Position control for slow dynamic systems: Haptic feedback makes system constraints tangible*, Conference Proceedings - IEEE International Conference on Systems, Man and Cybernetics, 2014-Janua (2014), pp. 3990–3995.

[48] H. Zheng, J. Hu, and Y. Liu, *A bilateral control scheme for vehicle steer-by-wire system with road feel and steering controller design*, Transactions of the Institute of Measurement and Control, 41 (2019), pp. 593–604.